

**COAXIAL PROBE FOR HIGH TEMPERATURE
DIELECTRIC CHARACTERIZATION**

by

Michael Dante Grady

A thesis submitted to the Graduate Faculty of
Auburn University
in partial fulfillment of the
requirements for the Degree of
Master of Science

Auburn, Alabama
August 9, 2010

Keywords: open-ended coaxial probe, spring-loaded probe
high temperature measurement, reflection coefficient, permittivity

Copyright 2010 by Michael Dante Grady

Approved by

Stuart Wentworth, Chair, Associate Professor of Electrical Engineering
Robert Dean, Assistant Professor of Electrical Engineering
Hulya Kirkici, Associate Professor of Electrical Engineering
Lloyd Riggs, Professor of Electrical Engineering

ABSTRACT

Wireless technologies have become an integral part in how we coexist on a daily basis. Specifically, the use of antenna systems plays a huge role in our daily lives. These antenna systems are largely used in some form for most all modern day cellular and radar applications. For proper construction of antenna systems, the electromagnetic properties of the material surrounding the antennas, in particular, the material's complex permittivity and permeability, must be thoroughly known. It is also important to note that the antennas will be subject to diverse temperature environments, so it is beneficial to know how the antenna material's electromagnetic properties will change with temperature.

This thesis describes the design and construction of a spring-loaded stainless steel open-ended coaxial probe used to find the electromagnetic properties of materials at elevated temperatures. This research uses network analyzer measurements of the reflection coefficient on an open-ended coaxial sensor in contact with a material. Permittivity is then extracted from the reflection coefficient data by the use of a lumped equivalent circuit model of the sensor's fields fringing into a sample. Computer verification of the technique is demonstrated, and results for two materials at a frequency range between 0.5 GHz - 1.8 GHz are measured at room temperature, 45 °C, 75 °C, and 100 °C.

ACKNOWLEDGMENTS

I would first like to give thanks to our Lord and savior because without him this would not have been possible.

To my mother, Vanessa Grady, sister, Vanesia Grady, and father, Samuel Adams, for believing in the youngest child.

To the rest of my family and friends for encouraging and helping me out in my times of need.

To my advisor, Dr. Stuart Wentworth, for his motivating teaching style and giving me this opportunity to contribute to the academic community.

To my Thesis Committee for their input and also helping make this transition a smooth one.

To Dr. Overtoun Jenda, Dr. Florence Holland, and the NSF Bridge to Doctorate Fellowship for providing a means for me to have a support system and excel throughout my Masters education.

To Dr. Shirley Scott-Harris for putting up with me for all these years and genuinely caring about my future.

To Calvin Cutshaw, Mike Palmer, Jim Lowry, and Linda Baressi for helping with the fabrication of our coaxial probe.

And lastly, to anyone else I may have forgotten while writing this.....Thank you!

TABLE OF CONTENTS

ABSTRACT	ii
ACKNOWLEDGMENTS	iii
LIST OF TABLES	viii
LIST OF FIGURES.....	ix
CHAPTER 1: INTRODUCTION	1
1.1 Motivation.....	1
1.2 Survey of Measurement Techniques.....	2
1.2.1 Freespace.....	2
1.2.2 Transmission Line.....	3
1.2.3 Resonant Cavity	4
1.2.4 Parallel Plate	5
1.2.5 Coaxial Probe.....	6
1.3 Open-Ended Coaxial Probe for Elevated Temperature Measurements	6
1.4 Presented Coaxial Probes.....	7
1.4.1 RF Coaxial Connector Test Probe	8
1.4.2 Stainless Steel Probe	8
1.4.3 Spring-loaded Stainless Steel Probe	8
1.5 Looking Ahead.....	9
CHAPTER 2: OPEN-ENDED COAXIAL PROBE THEORY	10

2.1 Lumped Equivalent Circuit Model	11
2.1.1 Importance of Reference Material in the Lumped Equivalent Circuit Model	15
2.1.2 Finding capacitances in the probe and sample.....	15
CHAPTER 3: TECHNIQUE VERIFICATION	17
3.1 Computer Results.....	17
CHAPTER 4: COAXIAL PROBES	21
4.1 RF Coaxial Connector Test Probe	21
4.1.1 Fabrication of RF Coaxial Connector Test Probe.....	22
4.1.2 RF Coaxial Connector Test Probe Geometry	23
4.1.3 RF Coaxial Connector Test Probe Room Temperature Setup	24
4.1.4 Calibration of RF Coaxial Connector Test Probe	25
4.1.5 Measured Results from RF Coaxial Connector Test Probe	27
4.1.6 Repeatability of Measurement Procedure	31
4.1.7 Motivation of RF Coax Connector Test Probe Measurements on SS Probe	32
4.2 Stainless Steel Probe	33
4.2.1 Stainless Steel Probe for Elevated Temperature Measurements.....	33
4.2.2 Construction of Stainless Steel Probe	34
4.2.3 Stainless Steel Probe Geometry	35
4.2.4 Stainless Steel Probe Room Temperature Setup.....	35
4.2.5 Calibration of the Stainless Steel Probe.....	37
4.2.6 Measured Results from Stainless Steel Probe.....	37

4.2.7 Motivation of Stainless Steel Probe Measurements on Spring-loaded Stainless Steel Probe	38
4.3 Spring-loaded Stainless Steel Probe	39
4.3.1 Construction of Spring-loaded Stainless Steel Coaxial Probe	39
4.3.2 Spring-loaded Stainless Steel Coaxial Probe Geometry	41
4.3.3 Spring-loaded Stainless Steel Probe Room Temperature Setup	41
4.3.4 Calibration of the Spring-loaded Stainless Steel Probe	41
4.3.5 Measured Results from Spring-loaded Stainless Steel Probe	42
CHAPTER 5: COAXIAL PROBE FOR HIGH TEMPERATURE DIELECTRIC CHARACTERIZATION	45
5.1 Spring-loaded Stainless Steel Probe Elevated Temperature Setup	45
5.2 Calibration of the Spring-loaded Stainless Steel Probe for Elevated Temperatures.....	47
5.3 Measured Results from Spring-loaded Stainless Steel Probe for Elevated Temperatures.....	48
CHAPTER 6: CONCLUSIONS	54
6.1 Technique Summary	54
6.2 Future Work	55
6.2.1 Numeric solution for an open-ended coaxial probe	56
6.2.2 Calibration Standards.....	60
6.2.3 Gold Plated Probe	61
6.3 Conclusions.....	65

REFERENCES	66
APPENDIX A: CALIBRATION STANDARDS OVERVIEW.....	69
A.1 Open Calibration Standard.....	69
A.2 Short Calibration Standard.....	70
A.3 Load Calibration Standard	72
APPENDIX B: TECHNIQUE DETAILS	79
B.1 Room Temperature Measurement Procedure.....	79
B.2 Elevated Temperature Measurement Procedure	82
A.3 Load Calibration Standard	72
APPENDIX C: MATLAB CODE	87
C.1 Lump Equivalent Circuit Model Code	87
C.1.a 1-Port De-embedding Algorithm.....	89
C.2 Numerical Method Extraction Code	91

LIST OF TABLES

Table 3.1 Computer Simulation Measurement Schematic	20
Table 4.1 Test Probe Properties	24
Table 4.2 Relative Permittivity Value for Full S11 Calibration Material Combo (test probe)	28
Table 4.3 Relative Permittivity Value for Response Calibration (test probe)	30
Table 4.4 Stainless Steel Probe Properties.....	35
Table 4.5 Relative Permittivity Value for Calibration Material Combinations (SS probe).	37
Table 4.6 Spring-loaded Stainless Steel Probe Properties	41
Table 4.7 Relative Permittivity Value for Calibration Material Combinations (Spring- loaded).....	42
Table 4.8 Relative Permittivity Value for Response Calibration (Spring-loaded probe)	43
Table 5.1 Relative Permittivity Value for Full-S11 Calibration (SL probe)	49
Table 5.2 Relative Permittivity Value for Response Calibration (SL probe)	51
Table 6.1 Thermal and Electrical Conductivities of Gold and Stainless	61
Table 6.2 Calculations of Heat Conducted by Gold Plated probe	64

LIST OF FIGURES

Figure 1.1 Free-space pyramidal horn antennas measuring a material	3
Figure 1.2 Coaxial and waveguide transmission line	4
Figure 1.3 Rectangular waveguide cavity resonator.....	4
Figure 1.4 Parallel plate capacitor with air (left) and parallel plate capacitor with dielectric material (right)	5
Figure 1.5 Coaxial Probe made from RF connector	6
Figure 2.1 Cross-section of open-ended coaxial probe.....	10
Figure 2.2 Open-ended coaxial probe in contact with material (left) and lumped equivalent circuit model of an open-ended coaxial probe (right)	11
Figure 2.3 Cutoff wavelengths of the TM and TE modes in a coaxial line.....	12
Figure 2.4 Field distributions of the principal TEM and lower order TE and TM modes in a coaxial line	13
Figure 3.1 ADS Schematic of Calibration	18
Figure 3.2 ADS Schematic of Measurement Process	19
Figure 4.1 N _{Male} to SMA _{Male} RF coaxial adapter	22
Figure 4.2 RF coaxial test probe made from NMale to SMAMale RF coaxial adapter ...	22
Figure 4.3 Cross-section of a coaxial line.....	22
Figure 4.4 Agilent HP-4396B VNA	24
Figure 4.5 Measurement Materials for test probe at room temperature	25

Figure 4.6 Test probe placed against a material during extraction	25
Figure 4.7 Measured value of Polycarbonate using the “Short” Response Calibration (brass).....	31
Figure 4.8 Relative Permittivity Value (Real vs Imaginary) for Tivar of Eight Separate Measurements using the {Air, brass, 50 Ω AR} Calibration Combination....	32
Figure 4.9 Stainless Steel Probe.....	34
Figure 4.10 Measurement Materials for Stainless Steel Probe at room temperature	36
Figure 4.11 Stainless Steel probe held with gripper during extraction.....	36
Figure 4.12 Stainless Steel probe placed against a material during extraction.....	36
Figure 4.13 Makeup of Spring-loaded Stainless Steel Probe	39
Figure 4.14 Spring-loaded Stainless Steel Probe	40
Figure 4.15 Measured value of Polyethylene using the “Open” Response Calibration (air).....	44
Figure 5.1 Stainless Steel probe high temperature measurement setup.....	46
Figure 5.2 Stainless Steel probe placed against a material during high temperature testing	47
Figure 5.3 Relative Permittivity Extraction of Tivar at four temperatures using the Room Temperature Full S11 Calibration	50
Figure 5.4 Relative Permittivity Extraction of Teflon at four temperatures using the Room Temperature Full S11 Calibration	51
Figure 5.5 Relative Permittivity Extraction of Tivar at four temperatures using the Response Calibration.....	52

Figure 5.6 Relative Permittivity Extraction of Teflon at four temperatures using the Response Calibration.....	53
Figure 6.1 Open-ended coaxial probe in contact with material of relative complex permittivity, ϵ_r	57
Figure 6.2 The probe tip geometry defining Equation (2.8).	58
Figure A.1 Styrofoam brand rectangular sheet.....	70
Figure A.2 Brass plate.....	70
Figure A.3 Steel plate from rectangular waveguide	71
Figure A.4 Short Standard connected at end of coaxial connector plumbing	71
Figure A.5 Liquid used as Short Standard	72
Figure A.6 50 Ω Annular Resistor.....	73
Figure A.7 Annular resistor	74
Figure A.8 Load Standard connected at end of coaxial connector plumbing	77
Figure A.9 Liquid used as Load Standard	77
Figure A.10 Square Resistor.....	78

CHAPTER 1

INTRODUCTION

1.1 Motivation

Most modern day communication technology employs an antenna system within its overall system design. For example, cell phone base stations make use of several antennas mounted on a cell tower to transmit and receive wireless signals. Likewise, many radar systems achieve the transmission and reception of wireless signals with the use of an aboveground directional antenna. These communication infrastructures are very practical, but are extremely vulnerable to natural disasters, vandalism, and terrorism [1]. Due to the consequences resulting from an antenna's destruction, it is critical to find an alternative means for transmitting and receiving wireless signals.

Subsurface antenna systems for cellular and radar applications may provide a robust alternative to aboveground antennas. One type of subsurface antenna is the geotextile antenna, consisting of electrically conductive structures containing electronic transmission and reception materials within its fibers. For proper construction, the electromagnetic properties of the material surrounding the antennas, in particular, the material's complex permittivity and permeability, must be thoroughly known [1]. It is also important to note that the antennas will be subject to diverse temperature

environments, so it is beneficial to know how the antenna material's electromagnetic properties will change with temperature.

At present, most materials are characterized at room temperature, and there is rather limited data regarding how the electromagnetic properties change with high temperatures. This principal concern is the motivation for the presented work.

1.2 Survey of Measurement Techniques

There are five common measurement techniques used to find a material's complex permittivity and permeability [2]. Among these are the Free-space, Transmission line, and Resonant cavity methods which can be used to simultaneously calculate a material's permittivity and permeability. In contrast, the Parallel plate and Coaxial probe techniques are well suited to calculate the permittivity of a material. A brief description and illustration of each procedure is described below.

1.2.1 Free-space

The free-space method involves using measures of reflection and transmission to extract electrical and magnetic properties. Measurements can be taken using a vector network analyzer. As shown in Figure 1.1, this method makes use of horn antennas as transmitters and receivers on opposite sides of the material under test. The measured received signal allows calculation of permittivity [3]. The free-space method uses either a TRL (thru, reflect, line) or TRM (thru, reflect, match) calibration technique to remove reflection errors [3, 4]. This method can be used for a variety of frequency ranges. The limiting factor for the frequency range is the horn dimensions. A few advantages of this

method are that it requires no direct contact to the materials and there are no special machining requirements for the materials. These advantages therefore make it a good choice for high temperature measurements [5]. A few main drawbacks to this method are that it requires using a large cross sectional area of the material in order to achieve accurate results and that the frequency response is limited by the waveguide.

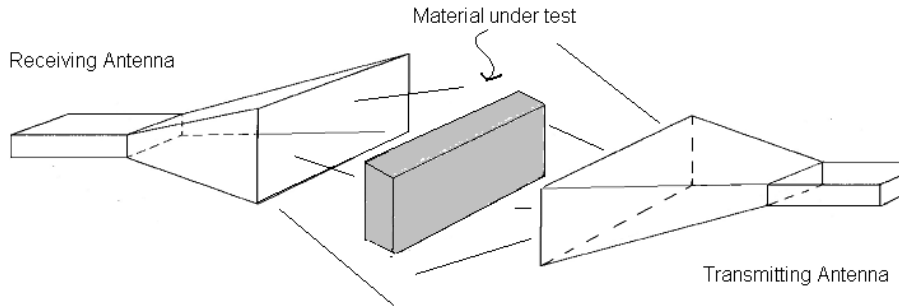


Figure 1.1 Free-space pyramidal horn antennas measuring a material

1.2.2 Transmission Line

The transmission line methods use reflection and transmission measurements to extract both electrical and magnetic properties, and are achieved by placing a material inside an enclosed segment of transmission line [3]. Measurements are taken with a network analyzer and either a coaxial line or a rectangular waveguide as depicted in Figure 1.2. The transmission line method can be executed by using either a one or two-port system. Coaxial lines and rectangular waveguides are primarily utilized when using a two port system. The one-port system involves placing a sample in a line terminated by a known load [6]. This transmission line method is widely regarded as one of the simpler ways to extract permittivity and permeability. This method can be used for a variety of

frequency ranges. The limiting factor for the frequency range is the transmission line dimensions. The key disadvantages to this method are that materials must be precisely machined to fit the test fixture, and air gaps at fixture walls will cause inaccuracies. Also, while coaxial line samples are harder to construct than waveguide samples, they can be used over a much wider frequency range.

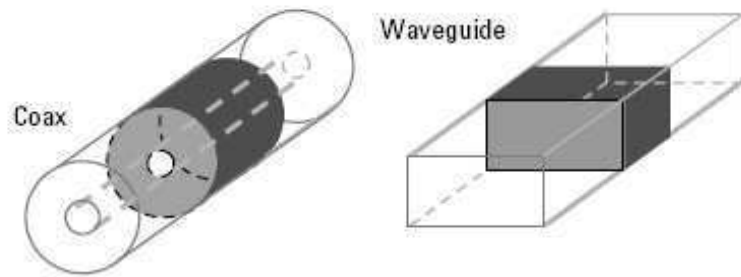


Figure 1.2 Coaxial and waveguide transmission line (Taken from [8])

1.2.3 Resonant Cavity

The resonant cavity method uses a cavity fixture to measure the quality factor and center frequency, parameters which are perturbed when a material is placed in the cavity. The changes in these values are then related to either or both the permittivity and permeability at a single frequency [3]. Measurements from the resonant cavity method can be taken with a network analyzer and stripline or waveguide resonator cavities. The stripline resonator cavity consists of a

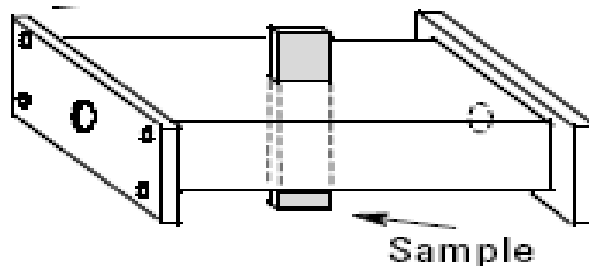


Figure 1.3 Rectangular waveguide cavity resonator (Taken from [8])

center-strip conductor mounted equidistantly between two ground planes and terminated by two end plates [7]. The waveguide resonator cavity can either be a rectangular (in Figure 1.3), circular, or elliptical waveguide terminated with plates at ends of the waveguide. This method can only be used for a single frequency. The limiting factor for this single frequency is the cavity dimensions. The resonant cavity method is considered to be the most accurate technique among techniques to find both electrical and magnetic properties. One disadvantage is that measurements can only be taken at a single frequency.

1.2.4 Parallel Plate

The parallel plate method involves using parallel plate capacitor theory. It consists of inserting a dielectric material in between two conducting plates [9]. When the sample is in the parallel plate arrangement, the capacitance is related exactly to the geometry and the permittivity [3].

Measurements are taken using a LCR

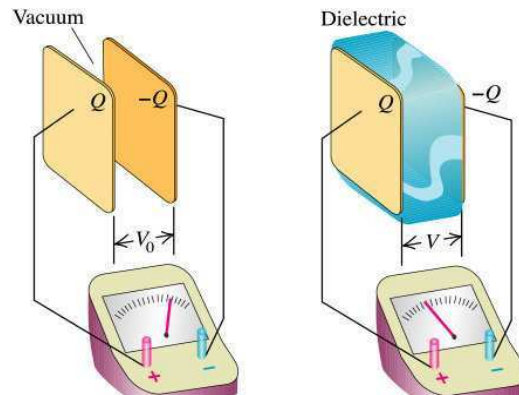


Figure 1.4 Parallel plate capacitor with air (left) and parallel plate capacitor with dielectric material (right) (Picture taken from <http://www.physics.sjsu.edu/...becker/physics51/capacitors.htm>)

meter or an impedance analyzer. Permittivity measurements can then be made by finding the ratio of the capacitance of the parallel plates with the space between the plates filled with the dielectric to the capacitance with the space being air [10] as depicted in Figure 1.4. The usable frequency range is determined by both the dimensions of the conducting

plate and the dimensions of the tested material. A few advantages to this method are its low-cost assembly and reasonably simple calculation of permittivity. This method is also well suited for thin flat materials. One main disadvantage to this method is that the charge density at the edges becomes larger as compared to the charge density in the center. This increased charge density causes the measured permittivity to appear larger than the actual value.

1.2.5 Coaxial Probe

The coaxial probe technique involves finding a material's permittivity by taking reflection coefficient measurements with an open-ended coaxial probe. The typical measurement system includes a network analyzer and a coaxial probe.



Figure 1.5 Coaxial Probe made from RF connector

The open-ended coaxial probe is a cut-off section of transmission line, as shown in Figure 1.5, which is brought in contact with the tested material such that the fields at the probe end fringe into the material. After the correct arrangement is achieved, the reflection data can then be related to permittivity because the fringing fields change as they come in contact with the tested material. This type of one-port measurement requires a three term calibration technique to ensure validity of acquired data. The usable frequency range is determined by both the dimensions of both the outer and inner conductors. The coaxial probe technique is suitable for taking measurements of multiple samples, liquids, and

planar solids. A few constraints to this method are that air gaps can cause significant errors, and it is not well-matched for materials with both electrical and magnetic losses. This technique is very attractive because of its non-destructive nature and the ease of sample preparation [3].

1.3 Open-Ended Coaxial Probe for Elevated Temperature Measurements

For robust, real world antenna design, it is beneficial to investigate how a material's electromagnetic properties change with temperature. In order to determine this, a measurement system that will withstand elevated temperatures must be developed. Open-ended coaxial probes are very attractive for taking high temperature measurements because the technique is a one-port measurement that does not require much sample preparation and offers a relatively simple user interface to an enclosed heating space. For this reason, an open-ended coaxial probe with properly selected fabrication materials is a superior measurement system for tackling the pre-stated problem. This work is demonstrated for temperatures up to 100°C.

1.4 Presented Coaxial Probes

In this work, three open-ended coaxial probes are presented. All probes are used to find the complex permittivity of dielectric materials at room temperatures, and one is used for elevated temperature measurements. The probes are brought in contact with the tested material such that the fields at the probe end fringe into the material. After this arrangement is formed, complex permittivity is then extracted. The first probe or test probe is made from a highly polished-machined RF coaxial connector. The second probe

(called the stainless steel probe) is made from a stainless steel rod and pipe and a RF Clamp Type Connector. The third probe or spring-loaded stainless steel probe is a variation of the original stainless steel probe designed for measurement at elevated temperatures. All measurements are taken for a frequency range of 0.5 GHz to 1.8 GHz.

1.4.1 RF Coaxial Connector Test Probe

The open-ended coaxial connector test probe was made from a highly polished-machined N_{Male} to SMA_{Male} RF coaxial connector. It is used to extract the complex permittivity of materials at room temperature. The RF coaxial connector test probe served as a baseline for the measurements taken. It was also the basis for the fabrication and testing of the stainless steel probe at room temperature.

1.4.2 Stainless Steel Probe

The stainless steel open-ended coaxial air probe is made from a stainless steel pipe and a stainless steel cylindrical rod connected to a RF N_{Male} Clamp Type Connector. The design and measurement results are compared with the room temperature measurement results obtained from the RF coaxial connector test probe. The weaknesses and measurement difficulty of this version of the stainless steel probe were the basis for the design and implementation of a spring- loaded coaxial probe.

1.4.3 Spring-loaded Stainless Steel Probe

This probe is a variation of the original stainless steel open-ended coaxial air probe which is made from a stainless steel pipe and a stainless steel cylindrical rod

connected to a RF N_{Male} Clamp Type Connector. This probe enhanced the original probe setup with the addition of a spring-loaded mechanism. It is ultimately used to extract the complex permittivity of materials at elevated temperatures. The spring-loaded stainless steel coaxial probe is demonstrated with temperatures as high as 100° C.

1.5 Looking Ahead

Chapter 2 describes the theory behind the open-ended coaxial probe method. The lumped equivalent circuit model of the probe's fields fringing into a sample modeling methods is presented. In Chapter 3, the open-ended coaxial probe technique is verified by computer simulation. Chapter 4 explains the construction, calibration, and measurement results obtained from the RF coaxial connector test probe. It alludes to how the acquired results motivate the construction and testing of the stainless steel coaxial probe. Chapter 4 also discusses the construction, calibration, and measurement results obtained from the stainless steel probe. It then describes how these results motivate the creation of a spring-loaded stainless steel coaxial probe. Lastly, Chapter 4 discusses the construction and calibration obtained from the spring-loaded stainless steel probe. The room temperature results obtained from the spring-loaded stainless steel coaxial probe are then explored. This chapter also tells about how the spring-loaded stainless steel coaxial probe will be used for high temperature measurements. In Chapter 5, the elevated temperature calibration and results are presented. These results are then compared to the room temperature results obtained from the spring-loaded stainless steel coaxial probe. Chapter 6 concludes with discussion on the advantages and disadvantages of each probe. This chapter also presents future improvements to the calibration and extraction procedures.

CHAPTER 2

OPEN-ENDED COAXIAL PROBE THEORY

The open-ended coaxial probe is a form of cut-off section of a transmission line that, like any other coaxial line, contains a center conductor of radius ‘ a ’ surrounded by some dielectric material with relative permittivity, ϵ_{rp} , all of which is enclosed by an outer conductor of radius ‘ b ’ as depicted in Figure 2.1. The expression “coaxial” comes from the inner and outer conductor sharing a common axis. Measurements from the coaxial probe are acquired by placing the end of the probe in contact with a material, so that the fields at the probe end fringe into the material and return reflection data measurements. The probe’s measured data presents a challenge in calculating the dielectric constant because there is no readily acknowledged analytical relationship between the reflection coefficient and permittivity.

There are several models for an open-ended coaxial probe. A number of these models give an expression for the admittance as a function of the dielectric constant. One of the most attractive modeling methods was employed: a lumped equivalent circuit

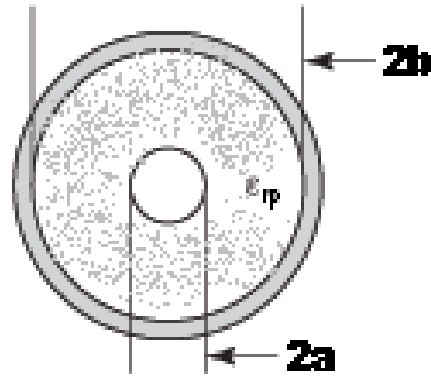


Figure 2.1 Cross-section of open-ended coaxial probe

model of the probe's fields fringing into a sample. This model is attractive because it is one of the simplest algorithms to implement.

2.1 Lumped Equivalent Circuit Model [12]

The lumped equivalent circuit model can be used when an open coaxial line, placed in contact with a test sample (Figure 2.2), is used as a sensor. The tested sample must be homogeneous within a volume sufficiently large to simulate a semi-infinite slab. A semi-infinite slab means that the tested sample thickness should allow the magnitude of the electric field at the far end of the sample to be at least two orders smaller than that at the probe to sample interface. If this condition is satisfied, the discontinuity at the termination of the coaxial line can be modeled by an equivalent lumped circuit. This discontinuity, in the absence of a lossy dielectric, is frequently assumed to be purely capacitive and to consist of two elements: a capacitance originating from the probe's fringing field (C_p), and a capacitance originating from the sample fringing field (C_s), as shown in Figure 2.2.

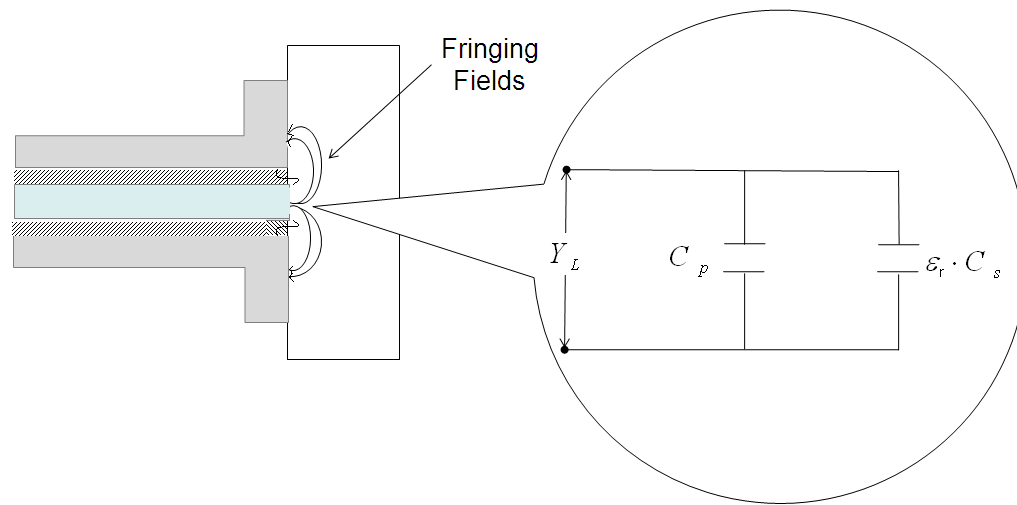


Figure 2.2 Open-ended coaxial probe in contact with material (left) and lumped equivalent circuit model of an open-ended coaxial probe (right)

This equivalent circuit is valid at frequencies where the dimensions of the line are small compared with the wavelength so that the open end of the line is not radiating and all the energy is concentrated in the fringe or reactive near field of the line. At higher frequencies, the value of the capacitance C_s increases with frequency, due to the increase in the evanescent TM modes being excited at the junction discontinuity [12]. The cutoff wavelength for the lowest-order TE mode and TM mode is shown in equation (2.1) and (2.2), respectively [11]. The cutoff wavelengths of the lower order TE and TM modes in a coaxial line are shown graphically in Figure 2.3. Figure 2.4 shows the field distributions of the principal TEM and lower order TE and TM modes in a coaxial line.

$$\lambda_{c_{TM_{01}}} \approx 2(b-a)\sqrt{\mu_{rp}\epsilon_{rp}} \quad (2.1)$$

$$\lambda_{c_{TE_{11}}} \approx \pi(b+a)\sqrt{\mu_{rp}\epsilon_{rp}} \quad (2.2)$$

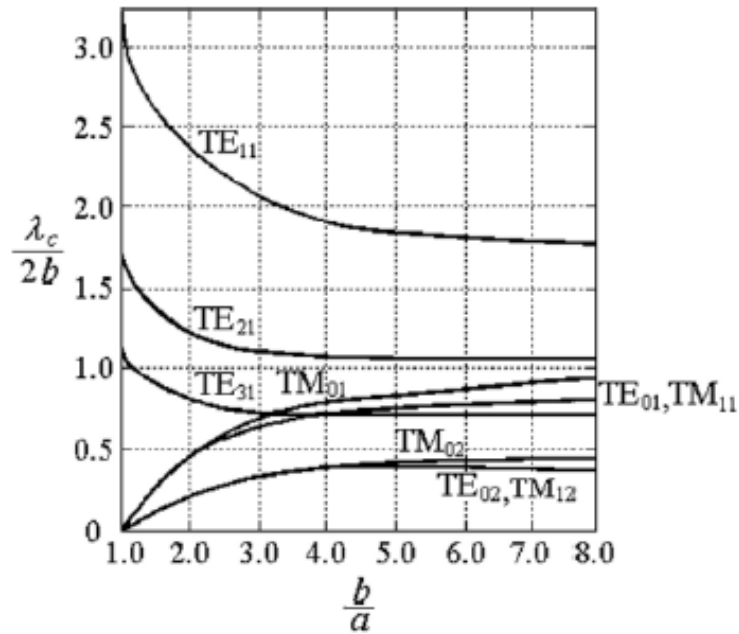


Figure 2.3 Cutoff wavelengths of the TM and TE modes in a coaxial line. (Taken from [11])

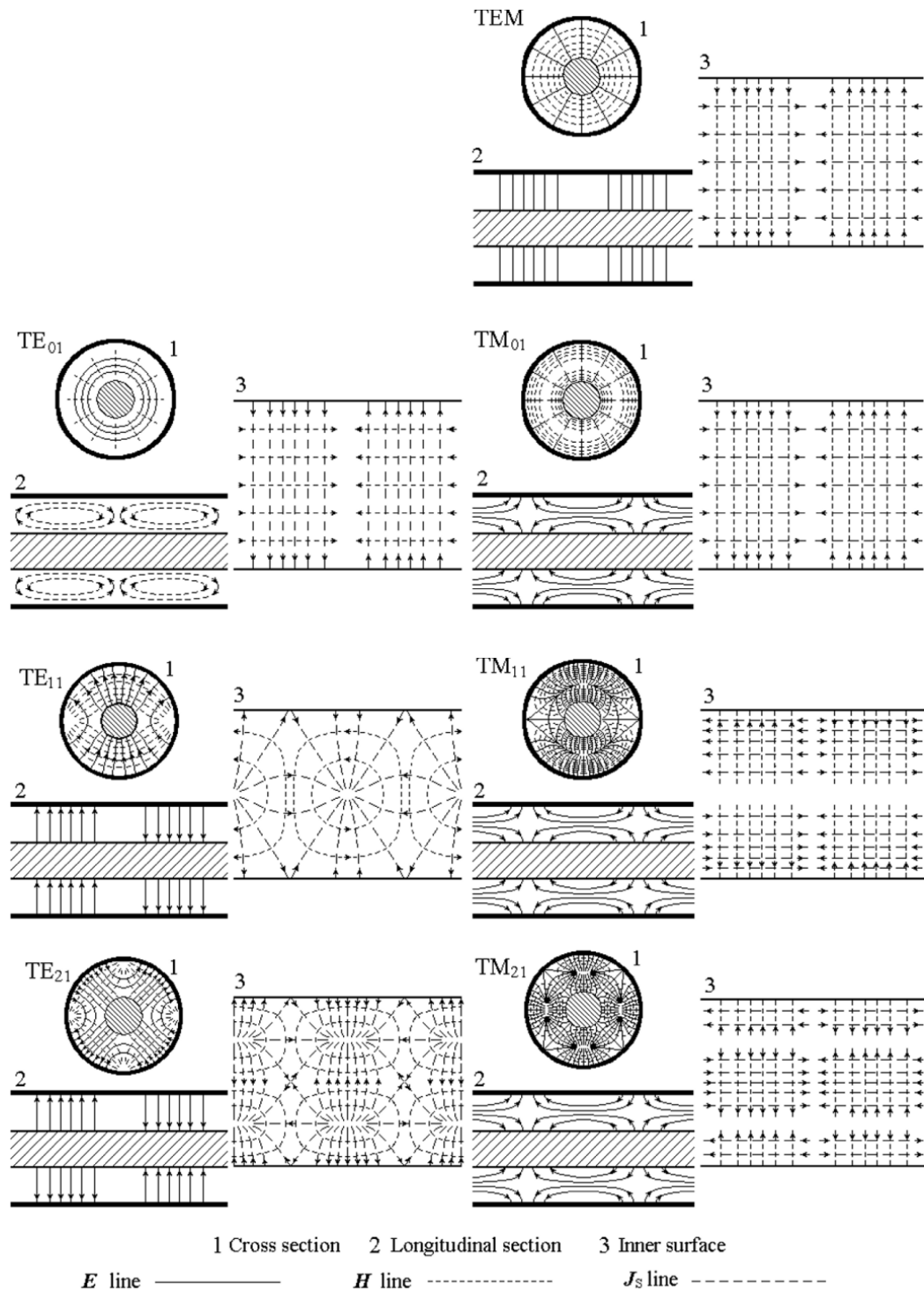


Figure 2.4 Field distributions of the principal TEM and lower order TE and TM modes in a coaxial line (Taken from [11])

The load admittance, Y_L , is given in terms of the voltage reflection coefficient, Γ^* , found at the end of an open-ended coaxial probe in contact with a dielectric medium with complex relative permittivity, ϵ_r , in equation (2.3).

$$Y_L = Y_o \cdot \frac{1 - \Gamma^*}{1 + \Gamma^*} \quad (2.3)$$

where Y_o is the characteristic admittance of the coaxial transmission line and Γ^* is the complex reflection coefficient.

In terms of the equivalent circuit model, the load admittance is,

$$Y_L = j\omega\epsilon_0 C_p + j\omega(\epsilon_r' - j\epsilon_r'')\epsilon_0 C_s \quad (2.4)$$

where ω is the angular frequency, C_p is the fringing capacitance into the probe and C_s is the fringing capacitance into the sample. Combining equations (2.3) and (2.4), we obtain

$$\epsilon_r' = \frac{-2 \cdot |\Gamma| \cdot \sin \theta}{\omega C_s Z_o (1 + 2 \cdot |\Gamma| \cdot \cos \theta + |\Gamma|^2)} - \frac{C_p}{C_s} \quad (2.5)$$

and

$$\epsilon_r'' = \frac{1 - |\Gamma|^2}{\omega C_s Z_o (1 + 2 \cdot |\Gamma| \cdot \cos \theta + |\Gamma|^2)} \quad (2.6)$$

where ϵ_r' , in (2.5), and ϵ_r'' , in (2.6), are the real part and the imaginary part of the relative complex permittivity, respectively, Z_0 is the characteristic impedance of the transmission line, and $|\Gamma|$ is the magnitude of the complex reflection coefficient with phase angle θ [12].

2.1.1 Importance of Reference Material in the Lumped Equivalent Circuit Model

Both the fringing capacitances in the probe, C_p , and the fringing capacitance in the sample, C_s , are found using a reference material. The dielectrics used for the reference material should be of known permittivity, should not be a calibration standard, and should satisfy the optimum capacitance condition at a selected measurement frequency (found in [13]). The calibration standards cannot be used as a reference material because the standards are used in the error correction model as an open, a short, or a load. If any standard is used as a reference material, this would result in a minimal change in the magnitude and phase of the reflection coefficient obtained for the reference material, and would result in systematic errors.

2.1.2 Finding capacitances in the probe and sample [13]

As a first approximation C_p can be assumed to be equal to zero, and either ϵ_r' or ϵ_r'' of the reference material can be used to determine C_s . The following relationships are employed, the first for ϵ_r' in equation (2.7) and the second for ϵ_r'' in equation (2.8):

$$C_s = \frac{-2 \cdot |\Gamma_{ref}| \cdot \sin \theta_{ref}}{\omega Z_o \epsilon_r' (1 + 2 \cdot |\Gamma_{ref}| \cdot \cos \theta_{ref} + |\Gamma_{ref}|^2)} \quad (2.7)$$

or

$$C_s = \frac{1 - 2 \cdot |\Gamma_{ref}|}{\omega Z_o \epsilon_r'' (1 + 2 \cdot |\Gamma_{ref}| \cdot \cos \theta_{ref} + |\Gamma_{ref}|^2)} \quad (2.8)$$

C_p in equation (2.9) can be found by rearranging equation (2.5):

$$C_p = \frac{-2 \cdot |\Gamma_{ref}| \cdot \sin \theta_{ref}}{\omega Z_o (1 + 2 \cdot |\Gamma_{ref}| \cdot \cos \theta_{ref} + |\Gamma_{ref}|^2)} - C_s \epsilon_r'. \quad (2.9)$$

where $|\Gamma_{ref}|$ is the magnitude of the complex reflection coefficient of the reference material with phase angle θ_{ref} .

The equivalent circuit model is most accurate for the following conditions: (i) C_p and C_s are independent of sample complex permittivity, (ii) C_p and C_s are independent of frequency, and (iii) the probe does not launch propagating radiation (i.e. it does not behave as an antenna). It is important to note that if the probe does behave as an antenna, it then falls under the propagating/radiation lumped equivalent circuit model described in [14] and [15].

CHAPTER 3

TECHNIQUE VERIFICATION

The extraction procedure was initially verified using Agilent Advance Design System (ADS). The open-ended coaxial probe setup was modeled for the materials that would eventually be tested at room temperature. Once verified with the computer results, the procedure was used with the data gathered from an HP 4326B vector network analyzer.

3.1 Computer Results

The simulation in Agilent's ADS was set up in same manner it would be used in an actual measurement. It must first be established that there are three different methods for which to calibrate the coaxial probe. One is to use an automatic calibration, where the calibration is done entirely by the VNA. Another is a semi-automatic calibration, where the VNA is used to calibrate the probe and then a de-embedding procedure is applied to obtain measurements. The last is a manual calibration, where the user manually measures each calibration standard and uses a de-embedding procedure to extract data. This simulation was done assuming a one-port manual calibration technique because the de-embedding procedure is ideally identical to the extraction method used in the automatic calibration. Data was taken from the end of an open-ended coaxial probe from a

reference material, a material under test, an open calibration standard, a short calibration standard, and a load calibration standard. Figure 3.1 shows the general layout of the calibration procedure while Figure 3.2 shows the ADS layout of the measurement procedure. The open-ended coaxial probe is connected to an S-parameter measurement termination and the respective measurement load. The measurement termination represents the reference plane at the VNA. In Figure 3.1, the “Open” impedance is equal to ∞ , the “Short” has an impedance of 0Ω , and the “Load” has an impedance of 50Ω .

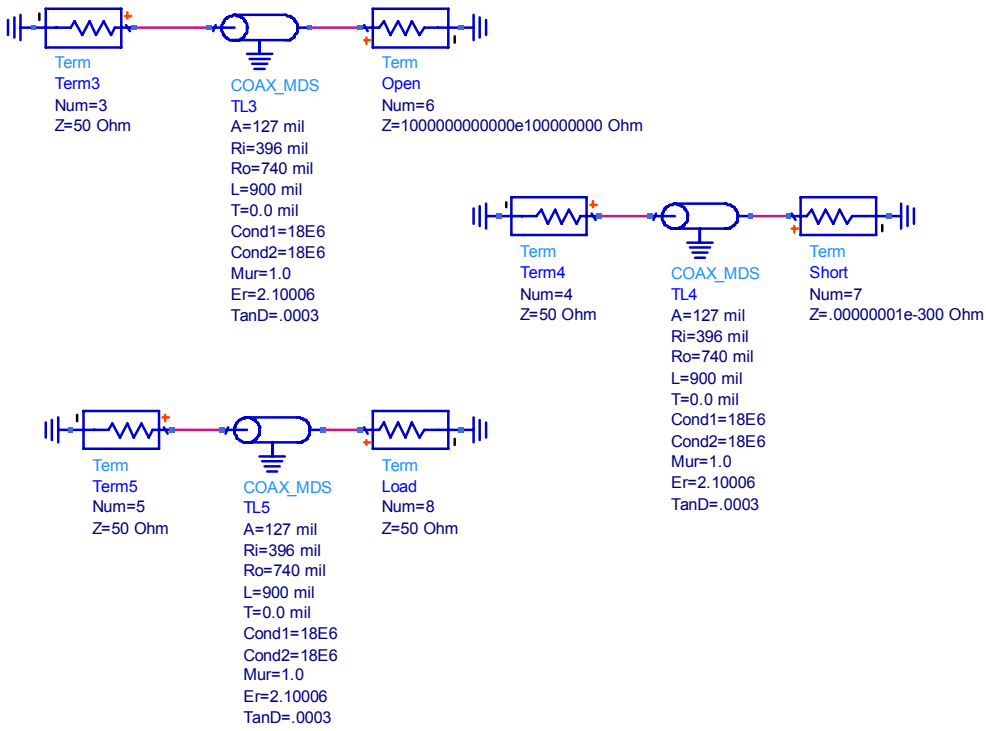


Figure 3.1 ADS Schematic of Calibration

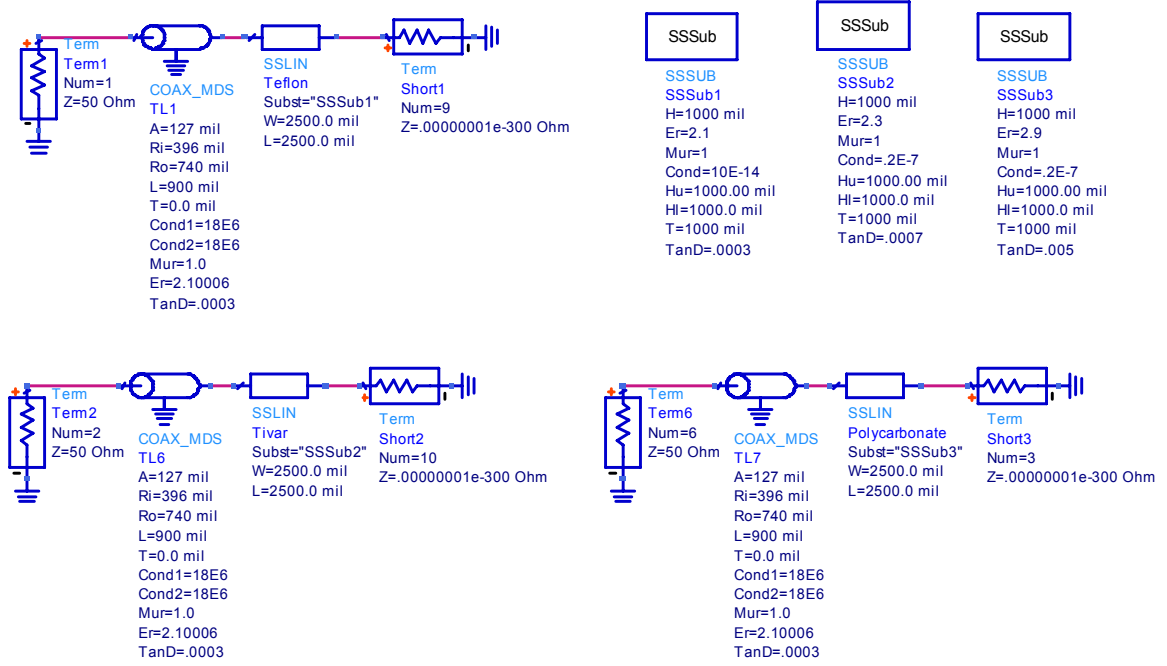


Figure 3.2 ADS Schematic of Measurement Process

In Figure 3.2, the probe first measures the reference material, Teflon with an ϵ_r value of 2.1 - $j0.0003$ [16], then two tested materials, Tivar with an ϵ_r value around 2.25 - $j0.0007$ [16] and Polycarbonate with an ϵ_r value around 2.85 - $j0.003$ [17]. The ADS coaxial line component, COAX_MDS, serves as the open-ended coaxial probe with the same geometry as the probe that will be used. The SSLIN is an ADS substrate component serving as the material to be tested by the coaxial line. Each substrate component is made to appear as a semi-infinite slab (by making the material thickness large as compared to the coaxial line size) with identical dielectric properties of the material it represents. Table 3.1 shows the calculated median values of ϵ_r from 500 MHz to 1.8 GHz for two different material input values.

Table 3.1 Computer Simulation Measurement Schematic

	Tivar		Polycarbonate	
	ϵ_r'	ϵ_r''	ϵ_r'	ϵ_r''
Input	2.300	0.0007	2.900	0.0050
Calculated	2.282	-2.652 E-16	2.831	-8.126 E-16

This ADS simulation confirms that this procedure indeed works. It can be seen that there is little difference in real component of the relative permittivity between the input and the calculated simulation values using the lumped equivalent circuit model from Chapter 2.1. It is also expected from this simulation that the one port measurement is not well suited for loss tangent measurements (imaginary component of the relative permittivity).

CHAPTER 4

COAXIAL PROBES

In this work, three open-ended coaxial probes are presented. All probes are used to find the complex permittivity of dielectric materials at room temperatures, and one is used for elevated temperature measurements. The probes are brought in contact with the tested material such that the fields at the probe end fringe into the material. After this arrangement is formed, complex permittivity is then extracted. The first probe or test probe is made from a highly polished- machined RF coaxial connector. The second probe or stainless steel probe is made from stainless steel bars and a RF Clamp Type Connector. The third probe or spring-loaded stainless steel probe is a variation of the original stainless steel probe. All measurements are within a frequency range of 0.5 GHz to 1.8 GHz.

4.1 RF Coaxial Connector Test Probe

The test probe for room temperature measurements was made from a highly polished-machined N_{Male} to SMA_{Male} RF coaxial connector. The N-Type coaxial connector proved to be a practical option for the initial test probe because the N-Type connector was manufactured with a characteristic impedance of 50 Ω (which is needed to match the measurement system). The design restrictions and measurement results obtained from the RF coaxial connector test probe were used as the motivation for the

construction of the stainless steel coaxial probe. The results from the RF coaxial connector test probe were also used to confirm the validity of the results obtained from the stainless steel probe at room temperature.

4.1.1 Fabrication of RF Coaxial Connector Test Probe

The test probe was fabricated from an N_{Male} to SMA_{Male} RF coaxial adapter (Figure 4.1) which has a characteristic impedance of 50Ω . A lathe was used to both remove the outer shell of the coaxial connector and file down the center pin and surrounding shell until the insulating material was flush with both the inner and outer metal conductors. After achieving a flat surface, the probe end was polished using 400, 600, 1000, and 2000 grade sand paper. The finished surface of the RF coaxial connector test probe is shown in Figure 4.2.



Figure 4.1 N_{Male} to SMA_{Male} RF coaxial adapter



Figure 4.2 RF coaxial test probe made from N_{Male} to SMA_{Male} RF coaxial adapter

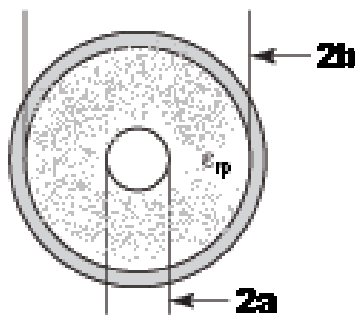


Figure 4.3 Cross-section of a coaxial line

4.1.2 RF Coaxial Connector Test Probe Geometry

The probe geometry was studied by finding the characteristics of a coaxial line in the form of Figure 4.3. The ratio between the outer diameter, b , and the inner diameter, a , determines the capacitance, C' , and inductance, L' , per unit length, and ultimately determines the characteristic impedance, Z_0 , as in equation (4.1).

$$Z_0 = \sqrt{\frac{L'}{C'}} = \frac{1}{2\pi} \sqrt{\frac{\mu_0 \mu_{rp}}{\epsilon_0 \epsilon_{rp}}} \ln\left(\frac{b}{a}\right) \quad [\Omega] \quad (4.1)$$

where

$$C' = \frac{2\pi\epsilon_0\epsilon_{rp}}{\ln\left(\frac{b}{a}\right)} \quad [\text{F/m}] \quad (4.2)$$

and

$$L' = \frac{\mu_0 \mu_{rp}}{2\pi} \ln\left(\frac{b}{a}\right) \quad [\text{H/m}] \quad (4.3)$$

where ϵ_{rp} is the relative permittivity of the insulating material, ϵ_0 is the permittivity of free space, μ_{rp} is the relative permeability of the insulating material (usually equal to 1), and μ_0 is the permeability of free space.

The characteristics of the room temperature probe are shown in Table 4.1.

Table 4.1 Test Probe Properties

Test Probe Properties		b	1.006 cm
		a	0.3226 cm
		ϵ_r	2.100 (Teflon)
	Z_0	47.05	Ω

4.1.3 RF Coaxial Connector Test Probe Room Temperature Setup

The RF coaxial connector test probe apparatus for room temperature measurements consists of an Agilent, Hewitt Packard-4396B Vector Network Analyzer (VNA) (Figure 4.4), the RF coaxial connector test probe, the calibration standards, the reference material,



Figure 4.4 Agilent HP-4396B VNA

and the material under test (Figure 4.5).

The Agilent HP-4396B VNA (description found at <http://www.testequipmentconnection.com>) provides RF vector network, spectrum, and optional impedance measurements for lab and production applications. Gain, phase, group delay, and distortion are some of the properties that can be measured using this one instrument. When combined with a test set, the Agilent 4396B provides reflection measurements, such as return loss, and SWR, and S parameters.

As a vector network analyzer, the Agilent 4396B operates from 100 kHz to 1.8 GHz with 1 mHz resolution, and its integrated synthesized source provides -60 to +20

dBm of output power with 0.1 dB resolution. The dynamic magnitude and phase accuracy are +/-0.05 dB and +/-0.3deg, so that it can accurately measure gain and group delay flatness.

The SMA test port of the HP 4396B VNA is connected to an open-ended coaxial probe. In order to extract proper measurements, the RF coaxial connector test probe must be placed firmly against the desired test sample, as seen in Figure 4.6.



Figure 4.5 Measurement Materials for test probe at room temperature

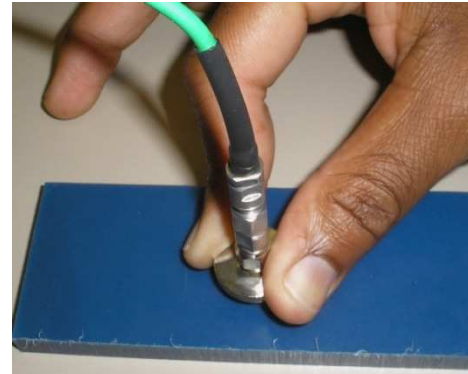


Figure 4.6 Test probe placed against a material during extraction

4.1.4 Calibration of RF Coaxial Connector Test Probe

The calibration of the RF coaxial connector test probe was accomplished by the use of either a three term “Full-S₁₁” calibration technique or a one term “Response” calibration. The “Full-S₁₁” method employed the use of an open, short, and matched load measured at the probe end. Theoretically, there are a wide variety of calibration material

combinations that may be employed for material measurement. The only restriction to calibration material (or calibration standard) usage depends on how well suited the calibration material is to the proposed probe. It is important to note that the proper selection of calibration materials for the probe is one of the most important aspects of obtaining accurate material measurement data. The “Response” method employed the use of either an open or a short measured at the probe end.

The geometry of the RF coaxial connector test probe is conducive to a variety of calibration material combinations. The following list highlights the materials utilized for the Open, Short, and Load calibration combinations:

- **Open** – air, Styrofoam
- **Short** - metal plate (brass), metal plate (steel), deionized water, distilled water, baking soda mixtures, Epsom salt mixtures, sea salt mixtures, table salt mixtures, and anti-freeze.
- **Load** - 50Ω annular resistor, deionized water, alcohol, anti-freeze, a 50Ω standard at the end of a chain of coaxial connector plumbing, and a resistive square print

Materials of known relative permittivity were used as references for testing the suitability of each calibration material combination. Descriptions of each calibration material can be found in Appendix A.

4.1.5 Measured Results from RF Coaxial Connector Test Probe

Two materials of known relative complex permittivity were used to verify the measurement capability of the RF coaxial connector test probe at 0.55 to 1.8 GHz: Polyethylene (Tivar) with an ϵ_r value around $2.25 - j0.0007$ [16] {other literature suggests an ϵ_r' of 2.3 [17]} and Polycarbonate with an ϵ_r value around $2.85 - j0.003$, found in [17] from the EM Properties of Materials Project at NIST Boulder {other literature suggests ϵ_r' of 2.9}.

A Teflon sample, with an ϵ_r value of $2.1 - j0.0003$, in [16], was used as the reference material for these measurements. Eight separate calibration and measurement data sets were taken for each calibration material combination. Table 4.2 shows the complex permittivity mean value for each corresponding “Full-S₁₁” calibration material combination. Table 4.3 shows the complex permittivity mean value for each corresponding “Response” calibration.

Table 4.2 Relative Permittivity Value for Full S_{11} Calibration Material Combo (test probe)

#	Full S_{11} - Calibration Material Combinations			PE		Polycarbonate	
	Open	Short	Load	ϵ'_r 2.3 (Stnd. Dev.)	ϵ''_r 0.0007 (Stnd. Dev.)	ϵ'_r 2.9 (Stnd. Dev.)	ϵ''_r 0.0050 (Stnd. Dev.)
1	Air	Metal (brass)	(a) 50 Ω Annular Resistor (AR)	2.310 (0.0072)	-0.0530 (0.1637)	2.704 (0.0237)	-0.2985 (0.1778)
			(b) Anti-freeze	2.302 (0.0425)	-0.8761 (0.2444)	2.606 (0.0184)	-1.820 (0.4915)
2	Air	Metal (steel)	(a) 50 Ω AR	2.317 (0.0092)	-0.0730 (0.1587)	2.753 (0.0121)	-0.3117 (0.0829)
			(b) Anti-freeze	2.305 (0.0094)	-1.105 (0.2811)	2.643 (0.0305)	-2.122 (0.5782)
			(c) Alcohol (90%)	2.359 (0.0114)	-2.159 (0.4852)	2.890 (0.0273)	-3.081 (0.7190)
			(d) Deionized water	2.112 (0.0064)	-0.9351 (0.3694)	2.124 (0.0196)	-1.388 (0.5360)
			(e) 50 Ω (plumbing)	2.333 (0.0045)	-0.1614 (0.0317)	2.745 (0.0080)	-0.2123 (0.0326)
3	Air	Distilled water	(a) 50 Ω AR	2.317 (0.0092)	0.3313 (0.3171)	2.703 (0.0315)	0.4145 (0.4349)
			(b) Anti-freeze	2.247 (0.0060)	-0.6825 (0.1406)	2.675 (0.0261)	-1.315 (0.2630)
4	Air	Deionized (DI) water	(a) 50 Ω AR	2.323 (0.0120)	0.3305 (0.3200)	2.734 (0.0351)	0.4293 (0.4503)
			(b) Anti-freeze	2.274 (0.0087)	-0.6510 (0.1331)	2.692 (0.0287)	-1.385 (0.2784)
			(c) Alcohol (90%)	2.354 (0.0113)	-1.783 (0.3453)	2.900 (0.0196)	-2.613 (0.5225)
5	Styro foam	Metal (steel)	(a) 50 Ω AR	2.317 (0.0055)	-0.1639 (0.1331)	2.737 (0.0137)	-0.3060 (0.0807)
			(e) 50 Ω Standard (plumbing)	2.345 (0.0059)	-0.1197 (0.0232)	2.662 (0.0064)	-0.1699 (0.0258)
			(f) Square Resistor	2.244 (0.0121)	-0.1158 (0.0576)	2.508 (0.0336)	-0.1722 (0.0786)
6	Styro foam	Short Stnd. (plumbing)	(a) 50 Ω Stand. (plumbing)	2.352 (0.0075)	-0.0832 (0.0197)	2.777 (0.0079)	-0.1341 (0.0214)

It can be seen from Table 4.2 that when using the $50\text{-}\Omega$ annular resistor as the load standard, the best calibration material combinations are #'s 2(a) and 4(a). This load standard appears to be the best all around load that can be used for the RF coaxial connector probe. In contrast, the $50\ \Omega$ commercial standard connected at the end of a chain of coaxial connector plumbing works best when combined with the short standard connected at the end of a chain of coaxial connector plumbing. This can be attributed to accuracy of the pre-calibrated manufactured standards. Also, when using anti-freeze as the load standard, the best calibration material combinations are #'s 3(b) and 4(b). It is expected that the measured values, when using anti-freeze as a load, exhibit error because anti-freeze is not well matched to the $50\ \Omega$ characteristic impedance load as it is used for. It can also be noticed that when alcohol is used as the load standard, measurement values are more precise when using a liquid for the short standard. Also, Styrofoam, as an open standard, served well in the place of air. This is also expected because Styrofoam is composed of mostly air with a ϵ_r' of 1.03. The RF coaxial connector probe is a good choice for obtaining room temperature measurements, but offers a few problems when attempting to maintain a planar fit against measurement materials. It can be observed that this one port measurement is not well suited for loss tangent measurements, unless extremely precise calibration standards can be used.

Table 4.3 Relative Permittivity Value for Response Calibration (test probe)

#	Response Calibration		PE		Polycarbonate	
			ϵ'_r 2.3 (<i>Stnd. Dev.</i>)	ϵ''_r 0.0007 (<i>Stnd. Dev.</i>)	ϵ'_r 2.9 (<i>Stnd. Dev.</i>)	ϵ''_r 0.0050 (<i>Stnd. Dev.</i>)
7	Short	(a)	Metal (brass)	2.383 <i>(X)</i>	0.9486 <i>(X)</i>	2.892 <i>(X)</i>
		(b)	Metal (steel)	2.372 <i>(X)</i>	-0.1808 <i>(X)</i>	2.837 <i>(X)</i>
8	Open	(a)	Air	2.347 <i>(0.0090)</i>	-0.0115 <i>(0.0283)</i>	2.788 <i>(0.0166)</i>
		(b)	Styrofoam	2.332 <i>(0.0114)</i>	0.0085 <i>(0.0318)</i>	2.778 <i>(0.0157)</i>

(X) – Standard deviation values are unusable due to abnormalities (Figure 4.7)

Table 4.3 shows that the “Open” Response calibration appears to more closely resemble the data obtained from the three term “Full-S₁₁” calibration. The “Open” Response calibration displays a relatively smooth output while the “Short” Response calibration exhibits inaccuracies at certain frequencies which make discovering the material’s actual value difficult. For the “Short” Response Calibration measurements, the relative complex permittivity median values were used due to the measurements exhibiting multiple abnormalities at multiple frequencies. These abnormalities compromise the standard deviation values as shown with Response calibration #7a, the measured value of Polycarbonate using the “Short” Response Calibration with brass (Figure 4.7). The abnormalities are assumed to be from the use of Response calibration materials that do not closely resemble the electromagnetic properties of the tested materials. The resemblance of calibration and tested materials during response calibration measurements are important because the Response measurement only has a one-term error model to

approximate with. For example, the reflection properties of air and Styrofoam resemble an open standard, while metal and water resemble a short standard.

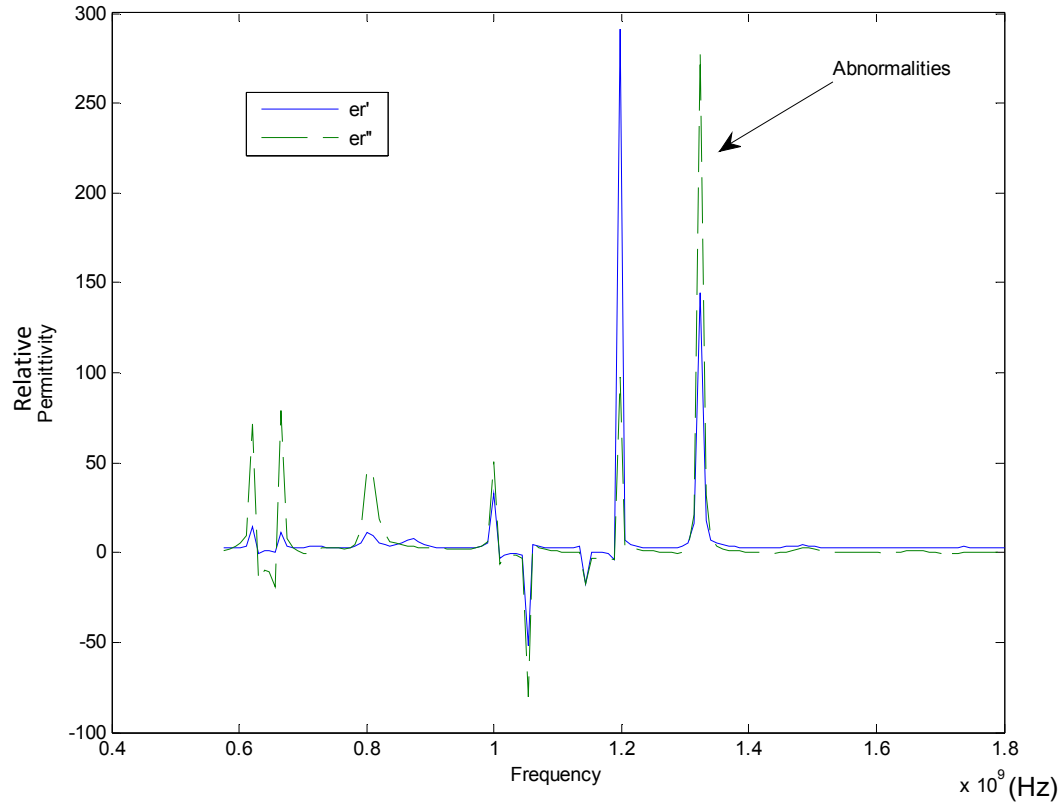


Figure 4.7 Measured value of Polycarbonate using the “Short” Response Calibration (brass)

4.1.6 Repeatability of Measurement Procedure

To study the repeatability of the general measurement procedure described in Chapter 4.1.3, the seven different room temperature Polyethylene measurements using calibration combination #1(a) are depicted. In Figure 4.8 a plot of the relative permittivity values (real vs. imaginary) of Tivar, extracted from the seven measurements taken, shows consistency in the results.

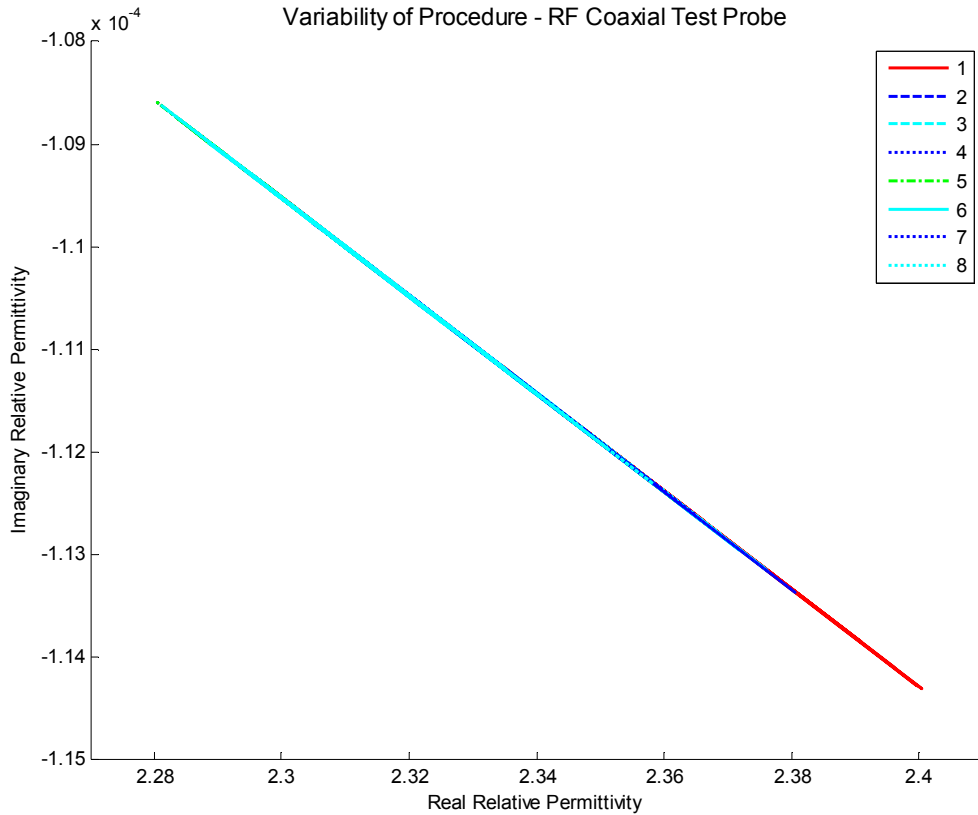


Figure 4.8 Relative Permittivity Value (Real vs Imaginary) for Tivar of Eight Separate Measurements using the {Air, brass, 50 Ω AR} Calibration Combination

4.1.7 Motivation of RF Coax Connector Test Probe Measurements on SS Probe

The results obtained from the RF coaxial connector test probe are used to validate the results obtained from the stainless steel probe at room temperature. Since the geometry of the stainless steel probe is not as user friendly as the RF Coaxial Connector Test Probe geometry, it is anticipated that certain calibration combinations will not be suitable for the stainless steel probe. Both the 50-Ω annular resistor and the 50-Ω from the coaxial plumbing as the load standard should be well-matched to be used with the stainless steel probe. Also, the alcohol standard should be well matched with the stainless steel probe because it is a liquid and should maintain a good contact with the probe.

Therefore, the calibration material combinations # 2(a), 2(c), 2(e), 4(c), 7, and 8 will be used to evaluate the room temperature performance of the stainless steel probe.

4.2 Stainless Steel Probe

The stainless steel probe was made from a stainless steel pipe and a stainless steel cylindrical rod connected to a RF N_{Male} Clamp Type Connector. The stainless steel probe assembly was based on the design restrictions and measurement results obtained from the RF coaxial connector test probe. The RF coaxial connector test probe provides a good means for material characterization at room temperature, but lacks the capability of providing an adequate means for material characterization at high temperatures- hence the need for a stainless steel probe for high temperature measurements. The results measured from the stainless steel probe at room temperature use the same calibration material combinations as the RF coaxial connector test probe. The results and design restrictions of the original stainless steel probe influenced the addition of a spring-loaded mechanism to combat the difficulties associated with the original stainless steel probe.

4.2.1 Stainless Steel Probe for Elevated Temperature Measurements

The stainless steel probe is used for elevated temperature measurements because it offers the user a means of quickly and easily obtaining material measurements at elevated temperatures. Stainless steel parts are readily available, and stainless steel has a low thermal conductivity, making it the preferred conductor material because it allows the user to comfortably hold one end of the probe while the other end is immersed in a heated environment.

4.2.2 Construction of Stainless Steel Probe

The construction of the stainless steel probe was based on the structure of the RF coaxial connector test probe. A one foot long stainless steel pipe used as the outer conductor and a stainless steel cylindrical rod used as the center conductor were electrically connected to an N-Male Clamp Type Connector on one end. In order to provide a snug fit inside the ferrule of the N-Male Clamp Type Connector, the tube was machined down, and a stainless steel washer was soldered to the opposite end of the pipe to provide a flange, which acts as an extended ground plane. The stainless steel rod was also soldered to the center pin. Three Teflon washers were then placed approximately 3 inches apart inside the stainless steel tube to provide a center positioned center conductor in reference to the outer conductor. After all parts formed a flanged open ended-coaxial probe, the probe end was machined flat and polished using 400, 600, 1000, and 2000 grade sand paper. The finished stainless steel probe is shown below in Figure 4.9.



Figure 4.9 Stainless Steel Probe

4.2.3 Stainless Steel Probe Geometry

The properties of the stainless steel coaxial probe are determined by using the same formulas of a coaxial cable at high frequencies, equation (4.1) - (4.3). The characteristics are listed in Table 4.4 as follows:

Table 4.4 Stainless Steel Probe Properties

Stainless Steel Probe Properties	b	1.011 cm
	a	0.3962 cm
	ϵ_r	1 (air)
Z ₀		56.15

4.2.4 Stainless Steel Probe Room Temperature Setup

The stainless steel probe room temperature measurement apparatus consists of a Vector Network Analyzer (VNA), the stainless steel probe, the calibration standards, the reference material, and the material under test (Figure 4.10).

The SMA test port of the HP 4396B VNA is connected to an open-ended stainless steel coaxial probe. In order to extract proper measurements, the stainless steel probe must be placed firmly against the desired test quantity. The shaft of this probe is approximately one foot long, so the user has the option to use a gripping apparatus (Figure 4.11) or manually hold the probe firmly at the probe tip (Figure 4.12).

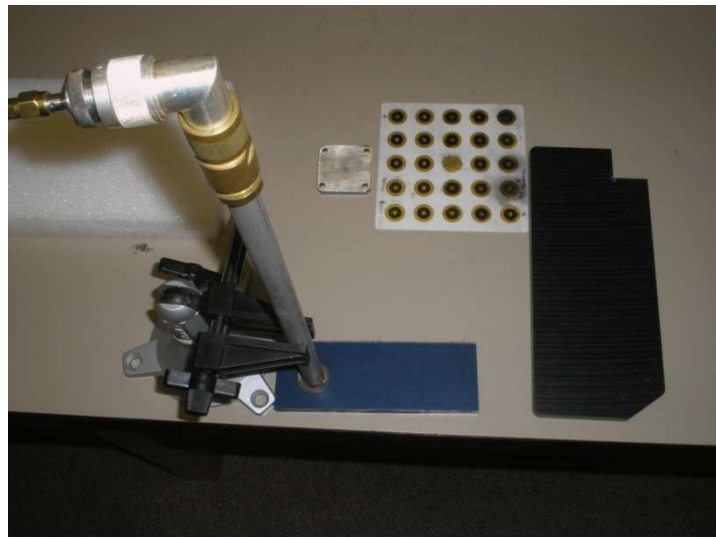


Figure 4.10 Measurement Materials for Stainless Steel Probe at room temperature

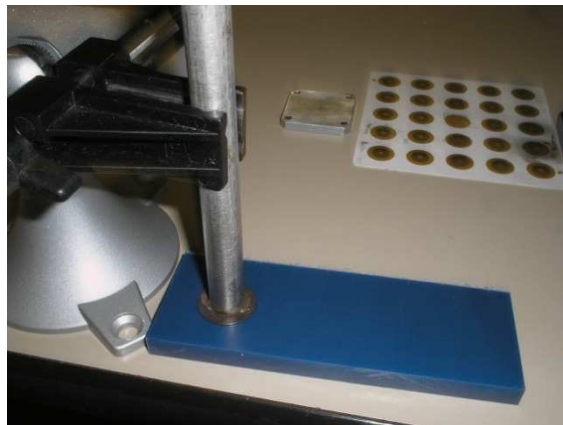


Figure 4.11 Stainless Steel probe held with gripper during extraction

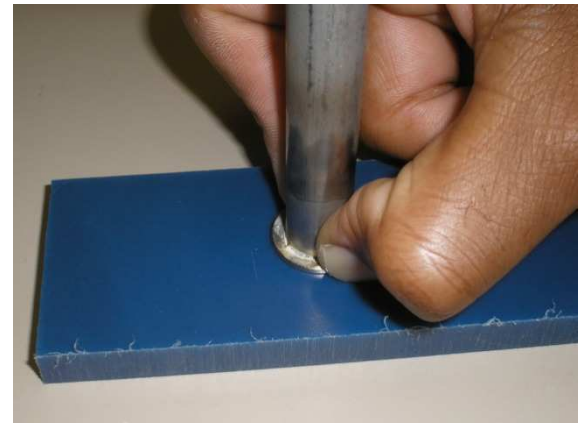


Figure 4.12 Stainless Steel probe placed against a material during extraction

4.2.5 Calibration of the Stainless Steel Probe

The calibration of the stainless steel probe was realized by the use of a three term “Full-S₁₁” calibration technique, identical to the calibration applied to the RF coaxial connector test probe in Chapter 4.1.4. Descriptions of each calibration material can be found in Appendix A.

4.2.6 Measured Results from Stainless Steel Probe

Tivar with an ϵ_r value of 2.3 - $j0.0007$, in [16], and Polycarbonate with an ϵ_r value of 2.9 - $j0.0003$, in [17], were used to verify the measurement capability of the stainless steel coaxial probe at 0.55 to 1.8 GHz. Teflon, with an ϵ_r value of 2.1 - $j0.0003$ [16], was used as the reference material. Eight separate calibration and measurement data sets were taken for each calibration material combination. Table 4.5 shows the complex permittivity mean value for each corresponding “Full-S₁₁” calibration material combination.

Table 4.5 Relative Permittivity Value for Calibration Material Combinations (SS probe)

#	Full S ₁₁ - Calibration Material Combinations			PE		Polycarbonate	
				ϵ'_r 2.3 (Stnd. Dev.)	ϵ''_r 0.0007 (Stnd. Dev.)	ϵ'_r 2.9 (Stnd. Dev.)	ϵ''_r 0.0050 (Stnd. Dev.)
2	Air	Metal (steel)	(a) 50 Ω AR	2.330 (0.0173)	-0.3407 (0.0686)	2.770 (0.0171)	-0.4748 (0.0958)
			(c) Alcohol (90%)	2.331 (0.0290)	-1.097 (0.3568)	2.690 (0.0664)	-1.661 (0.5634)
			(e) 50 Ω (plumbing)	2.341 (0.0569)	-0.0464 (0.2813)	2.741 (0.0958)	-0.0613 (0.3808)
4	Air	Deionized (DI) water	(c) Alcohol (90%)	Inconclusive, due to center conductor movement			

It can be seen that only four calibration material combinations were taken using the stainless steel probe. This was due to the difficulty presented in obtaining quality measurements with the stainless steel probe. The probe offers a challenge in maintaining a good planar fit to the material under test which limits the calibration usage. Even with the use of liquid calibration combinations, this probe made measurement extraction very difficult. The calibration material combination # 2(a) proved to be the best combination to use for the stainless steel probe. Calibration material combination # 4(c) appeared to be a good fit for this probe, but the data was unusable due to the erroneous center conductor movement of the stainless steel probe. This data confirms the need for a better built probe. The next logical progression is to find another method to test the validity of stainless steel probe.

4.2.7 Motivation of Stainless Steel Probe Measurements on Spring-loaded Stainless Steel Probe

The stainless steel probe presented the challenges of (1) maintaining a level contact plane between the center and outer conductor, (2) maintaining intimate contact among center conductor, outer conductor, and material under test, and (3) making an allowance for the center conductor altering its initial position after coming in contact with a material. These problems proved to amplify measurement difficulty which encouraged the addition of a spring-loaded mechanism to be added to the center conductor.

4.3 Spring-loaded Stainless Steel Probe

The spring-loaded stainless steel coaxial probe was an enhancement to the original stainless steel probe, with the major difference lying in a spring being inserted in between the center pin and the stainless steel rod used for the center conductor. The original stainless steel coaxial probe offered both a measurement difficulty and a challenge in assuring both the center and outer conductor maintained an intimate contact with the material under test. This probe also uses the same calibration material combinations as the two preceding coaxial probes for obtaining room temperature measurements. It is eventually used to obtain elevated temperature measurements.

4.3.1 Construction of Spring-loaded Stainless Steel Coaxial Probe

The construction of the spring-loaded stainless steel coaxial probe was motivated by the design restrictions associated with the original stainless steel probe. A stainless steel pipe used as the outer conductor and a stainless steel cylindrical rod used as the center conductor were electrically connected to an N-Male Clamp Type Connector on one end. In order to provide a snug fit inside the ferrule of the N-Male Clamp Type Connector, the tube was machined down and silver-filled epoxy was used to help provide a good electrical connection. A stainless steel washer was soldered to the opposite

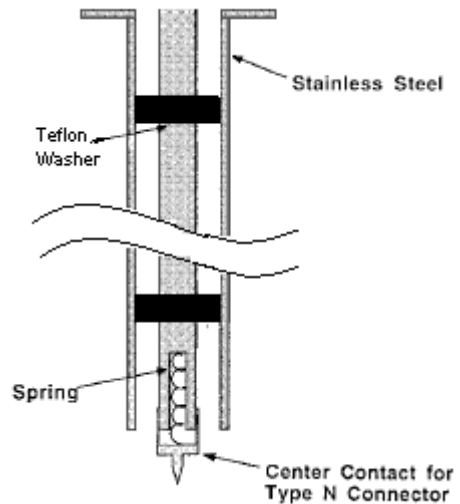


Figure 4.13 Makeup of Spring-loaded Stainless Steel Probe (modified from [18])

end of the pipe to provide a flange, which acts as an extended ground plane. The stainless steel rod was electrically connected to a stainless steel spring, on one end, which was also electrically connected to the center pin, on the other end, using a silver-filled epoxy. Two Teflon washers were then placed inside the stainless steel tube at both ends to provide a center positioned center conductor in reference to the outer conductor (Figure 4.13). The inner diameters of the washers were cut large enough such that the stainless steel center conductor could have an unobstructed-frictionless path to move through the washers. After all parts formed a flanged spring-loaded open ended-coaxial probe, the probe end was machined flat and polished using 400, 600, 1000, and 2000 grade sand paper. The finished stainless steel probe is shown below in Figure 4.14.

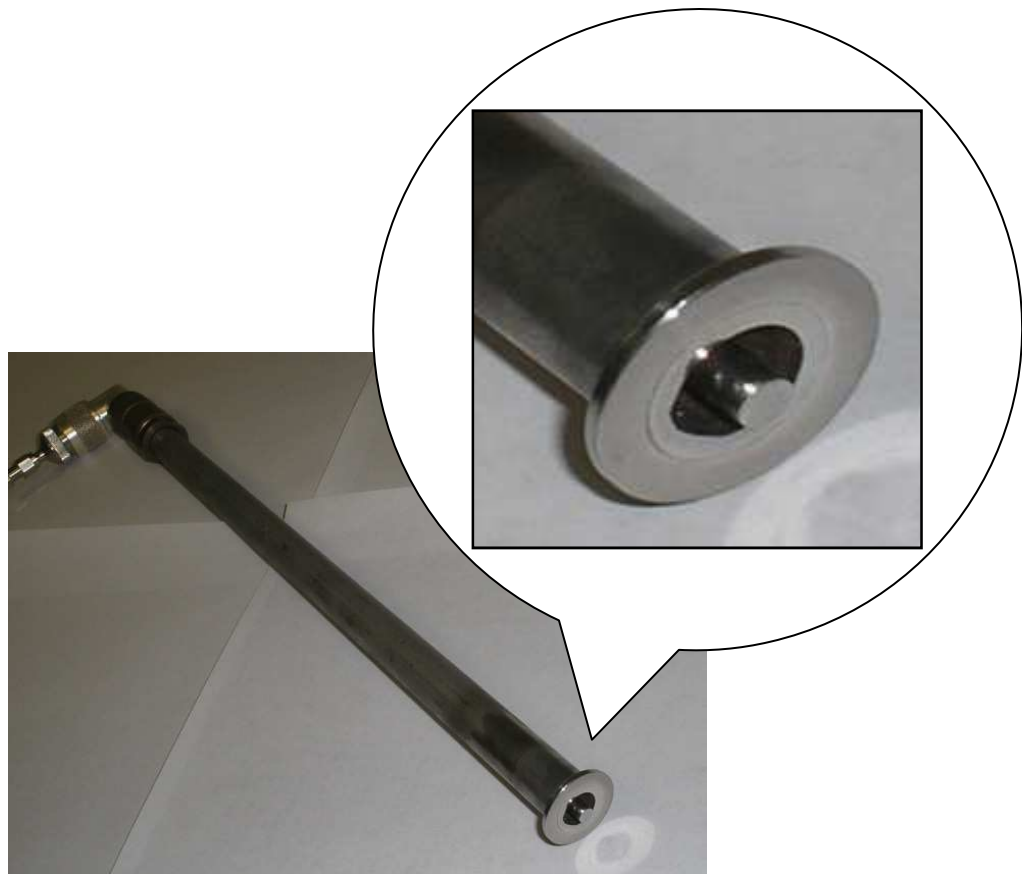


Figure 4.14 Spring-loaded Stainless Steel Probe

4.3.2 Spring-loaded Stainless Steel Coaxial Probe Geometry

The properties of the spring-loaded stainless steel coaxial probe are determined by using the same formulas of a coaxial cable at high frequencies, equation (4.1) - (4.3). The characteristics are listed in Table 4.6 as follows:

Table 4.6 Spring-loaded Stainless Steel Probe Properties

Spring-loaded SS Probe Properties	b	1.011 cm
	a	0.3962 cm
	ϵ_{rp}	1 (air)
Z₀	56.15	

4.3.3 Spring-loaded Stainless Steel Probe Room Temperature Setup

The spring-loaded stainless steel probe room temperature measurement set-up is identical to the measurement set-up of the stainless steel probe described in Chapter 4.2.4.

4.3.4 Calibration of the Spring-loaded Stainless Steel Probe

The calibration of the spring-loaded stainless steel probe was realized by the use of either a three term “Full-S₁₁” calibration technique or a one term “Response” calibration, identical to the calibration applied to the RF coaxial connector test probe in Chapter 4.1.4. The only restriction to the exact type of calibration combination that may be used is that the center conductor must be compressed. Descriptions of each calibration material can be found in Appendix A.

4.3.5 Measured Results from Spring-loaded Stainless Steel Probe

Tivar with an ϵ_r value of $2.3 - j0.0007$, in [16], and Polycarbonate with an ϵ_r value of $2.9 - j0.0003$, in [17], were used to verify the measurement capability of the stainless steel coaxial probe at 0.55 to 1.8 GHz. Teflon, with an ϵ_r value of $2.1 - j0.0003$ [16], was used as the reference material. Eight separate calibration and measurement data sets were taken for each calibration material combination. Table 4.7 shows the complex permittivity mean value for each corresponding “Full-S₁₁” calibration material combination. Table 4.8 shows the complex permittivity mean value for each corresponding “Response” calibration.

Table 4.7 Relative Permittivity Value for Calibration Material Combinations (Spring-loaded)

#	Full S ₁₁ - Calibration Material Combinations				PE		Polycarbonate	
					ϵ'_r 2.3 (Stnd. Dev.)	ϵ''_r 0.0007 (Stnd. Dev.)	ϵ'_r 2.9 (Stnd. Dev.)	ϵ''_r 0.0050 (Stnd. Dev.)
1	Air	Metal (steel)	(a)	50 Ω AR	2.787 (0.0490)	0.2362 (0.0479)	4.013 (0.1338)	-0.0443 (0.0324)
5	Styro foam	Metal (steel)	(a)	50 Ω AR	2.326 (0.0124)	-0.2361 (0.0559)	2.738 (0.0151)	-0.3281 (0.0825)
			(e)	50 Ω Stnd. (plumbing)	2.316 (0.0394)	-0.2028 (0.3888)	2.678 (0.1050)	-0.2970 (0.5322)
			(f)	Square Resistor	2.299 (0.0110)	-0.3345 (0.0541)	2.654 (0.0313)	-0.4862 (0.0722)
6	Styro foam	Short Stnd. (plumbing)	(a)	50 Ω Stnd. (plumbing)	2.341 (0.0390)	0.0984 (0.0455)	2.756 (0.0451)	0.6074 (0.2742)

The 50Ω annular resistor still proves to be the best option available for use as the “load” calibration standard. Also, the 50Ω commercial standard connected at the end of a chain of coaxial connector plumbing works well with the short standard connected at the end of a chain of coaxial connector plumbing. The use of air as the “open” calibration standard is not practical for use with the spring-loaded stainless steel probe because the electrical length and characteristic impedance both change when the spring is compressed versus being extended. The square resistor in theory would offer the best “load” calibration fit to this probe because of its large surface area, but the impedance mismatch is too high. If a square resistor with the proper 50Ω characteristic impedance is used, it is then expected to have comparable results, if not better, than the 50Ω annular resistor. The 50Ω annular resistor still offers the challenge of aligning the spring-loaded probe with the resistor’s metal contacts.

Table 4.8 Relative Permittivity Value for Response Calibration (Spring-loaded probe)

#	Response Calibration		PE		Polycarbonate	
			ϵ'_r 2.3 (<i>Stnd. Dev.</i>)	ϵ''_r 0.0007 (<i>Stnd. Dev.</i>)	ϵ'_r 2.9 (<i>Stnd. Dev.</i>)	ϵ''_r 0.0050 (<i>Stnd. Dev.</i>)
7	Short	(a)	Metal (brass)	2.065 (X)	-0.0494 (X)	2.001 (X)
		(b)	Metal (steel)	2.063 (X)	-0.0326 (X)	1.999 (X)
8	Open	(a)	Air	2.745 (X)	0.0715 (X)	3.916 (X)
		(b)	Styrofoam	2.317 (0.0430)	-0.0107 (0.0250)	2.744 (0.1157)

(X) – Standard deviation values are unusable due to abnormalities (Figure 4.15)

It can be seen from Table 4.8 that the “Open” Response calibration appears to more closely resemble the data obtained from the three term “Full-S₁₁” calibration. The “Open” Response calibration displays a relatively smooth output while the “Short” Response calibration exhibits abnormalities at certain frequencies which make discovering the material’s actual value difficult. The relative complex permittivity median values were used for the “Short” Response Calibration measurements because these abnormalities compromise the standard deviation values as shown with Response calibration #8a, the measured value of Polyethylene using the “Open” Response Calibration with air (Figure 4.15). The “Air” calibration exhibits error because the spring-loaded probe’s center conductor must be compressed in order to obtain accurate measurements as shown in Chapter 4.3.5.

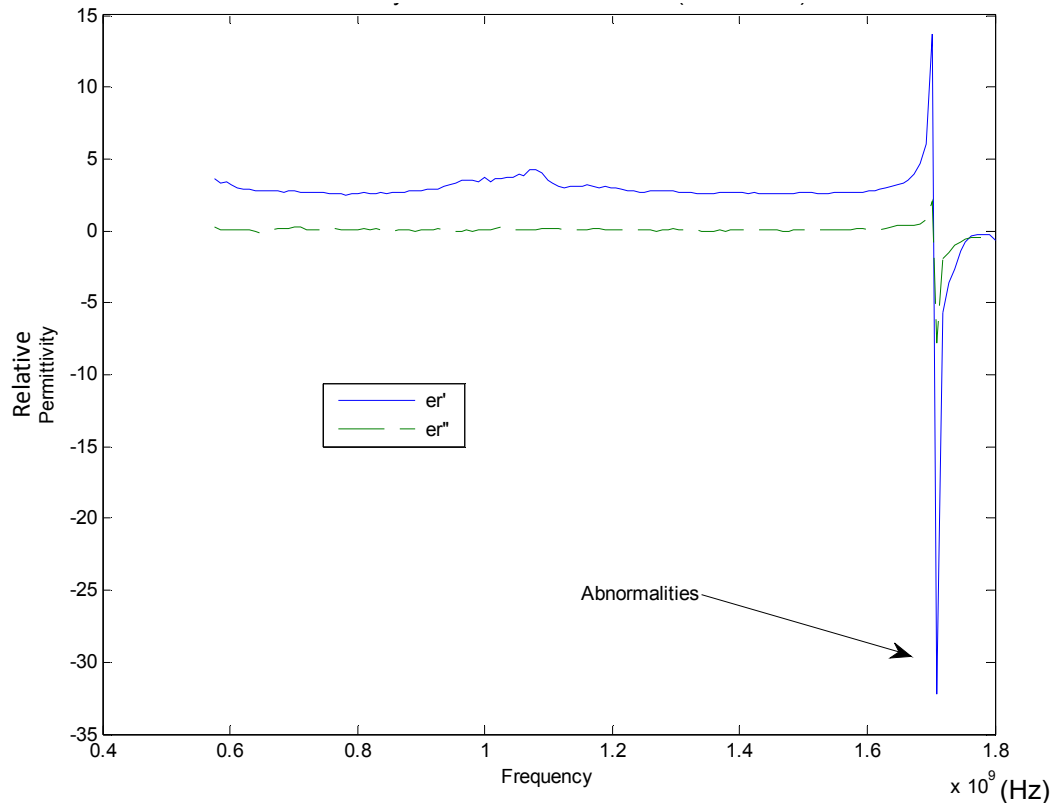


Figure 4.15 Measured value of Polyethylene using the “Open” Response Calibration (air)

CHAPTER 5

COAXIAL PROBE FOR HIGH TEMPERATURE DIELECTRIC CHARACTERIZATION

The spring-loaded stainless steel coaxial probe is used to extract material properties at elevated temperatures. It offers an advantage over standard open-ended coaxial probes by having a spring-loaded center conductor that forces an intimate contact with the material under test. It has been noted that if this connection is compromised, measurement results can be distorted by as high as 50% [19]. At elevated temperatures, the probe and material interface should be of sound contact and should not require any manual alterations, so as to not present any physical harm to the user.

5.1 Spring-loaded Stainless Steel Probe Elevated Temperature Setup

The spring-loaded stainless steel probe elevated temperature measurement set-up was done such that high temperature measurements could be taken safely and without damaging expensive equipment. The spring-loaded stainless steel coaxial probe elevated temperature measurement apparatus consists of a Vector Network Analyzer (VNA), a variable heating system (furnace), the spring-loaded stainless steel probe, the calibration standards, the reference material, and the material under test.

The SMA test port of the HP 4396B VNA is connected to an open-ended coaxial probe. An aluminum stopper is placed around the spring-loaded stainless steel probe and both are inserted inside overhead opening of furnace. A clamp is then placed around the aluminum stopper to control the probe's insertion distance (Figure 5.1). In order to extract proper measurements, the spring-loaded stainless steel probe must be placed firmly against the test sample surface. It is necessary to add a brick inside the furnace to ensure the material under test is at an acceptable elevation for testing (Figure 5.2).

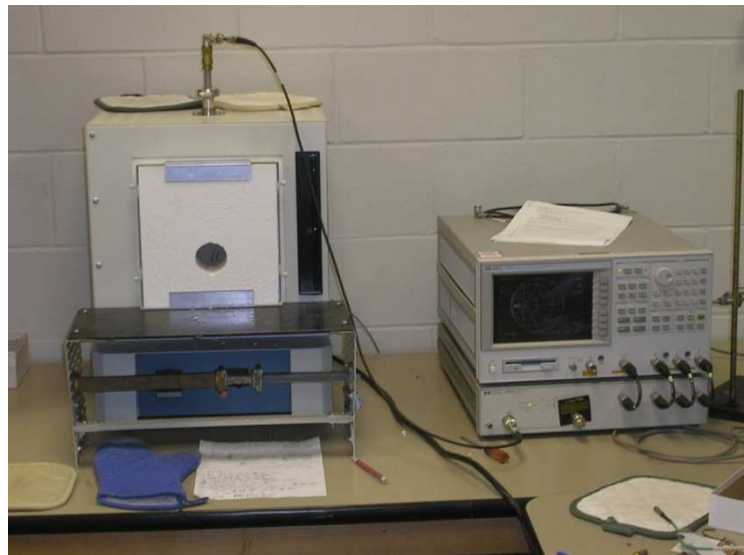


Figure 5.1 Stainless Steel probe high temperature measurement setup

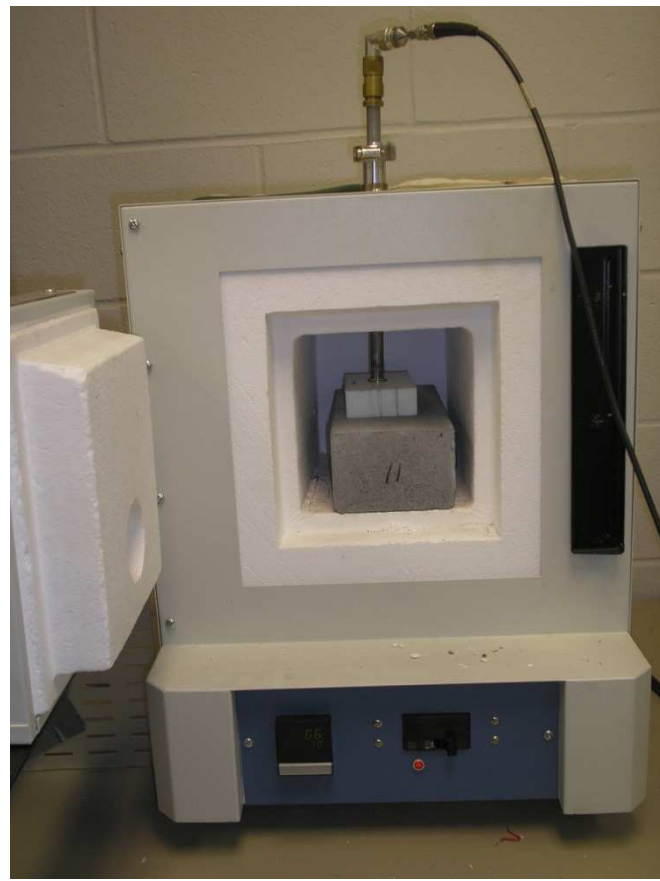


Figure 5.2 Stainless Steel probe placed against a material during high temperature testing

5.2 Calibration of the Spring-loaded Stainless Steel Probe for Elevated Temperatures

The calibration of the spring-loaded stainless steel probe was realized by the use of either a three term “Full-S₁₁” calibration technique or a one term “Response” calibration, identical to the calibration applied to the RF coaxial connector test probe in

Chapter 4.1.4. The only restriction to the exact type of calibration combination that may be used is that the center conductor must be compressed.

During the initial measurement stage, the probe was calibrated with the three term “Full-S₁₁” calibration technique {Styrofoam, Short Stand. (plumbing), 50 Ω Stand. (plumbing)}. The probe, material under test, and reference material were all calibrated at room temperature. The Styrofoam, short commercial standard connected at the end of a chain of coaxial connector plumbing, and 50 Ω commercial standard connected at the end of a chain of coaxial connector plumbing calibration was chosen because of the high repeatability of the manufactured calibration standards. For subsequent measurement stages, the one term “Response” calibration {Styrofoam} was used. For this calibration, the probe and material under test were at the measurement temperature, while reference material was at room temperature [20]. The one term “Response” method served to be the best possible calibration sequence for high temperatures because of the dangers associated with the calibration materials not being favorable for high temperature measurements. Descriptions of each calibration material can be found in Appendix A.

5.3 Measured Results from Spring-loaded Stainless Steel Probe for Elevated Temperatures

Teflon, with an ϵ_r value of $2.1 - j0.0003$ [16], and Tivar, with an ϵ_r value of $2.3 - j0.0007$, in [16], were used to verify the measurement capability of the spring-loaded stainless steel coaxial probe for elevated temperature measurements at 0.55 to 1.8 GHz. Teflon was used as the reference material. Table 5.1 shows the complex relative permittivity mean value for a room temperature “Full-S₁₁” calibration used to measure

the materials at each respective temperature. The Full-S₁₁ measurements were performed such that one room temperature calibration was performed, and the resulting measurements were performed at elevated temperatures. Table 5.2 shows the complex relative permittivity mean value for each corresponding “Response” calibration at the respective measurement temperature. The Response measurements were implemented such that a new calibration and measurement were performed at each respective temperature.

Table 5.1 Relative Permittivity Value for Full-S₁₁ Calibration (SL probe)

Full-S ₁₁ Calibration Styrofoam, Short Stnd. (plumbing), 50 Ω Stnd. (plumbing)				
Temp. (°C)	Teflon		Polyethylene	
(23)	ϵ'_{r} 2.1 (<i>Stnd. Dev.</i>)	ϵ''_{r} 0.0003 (<i>Stnd. Dev.</i>)	ϵ'_{r} 2.3 (<i>Stnd. Dev.</i>)	ϵ''_{r} 0.0007 (<i>Stnd. Dev.</i>)
23	2.11 (0.0203)	0.0492 (0.0925)	2.341 (0.0477)	0.0984 (0.1398)
45	2.258 (0.0329)	0.0660 (0.1106)	2.496 (0.0435)	0.0957 (0.1405)
75	2.318 (0.0321)	0.0690 (0.1165)	2.513 (0.0530)	0.0908 (0.1433)
100	2.338 (0.0310)	0.0650 (0.1184)	2.504 (0.0586)	0.0806 (0.1428)

The results from the “Full-S₁₁” calibration (Table 5.1) agree for the room temperature measurements, but start to exhibit error at higher temperatures. This increased error is a result of the “Full-S₁₁” calibration method not taking the effects of thermal expansion of the probe into account. Figure 5.3 and Figure 5.4 show a plot of the “Full-S₁₁” calibration measurements taken at elevated temperatures. The probe’s accuracy farther decreases as

the characteristic impedance of the probe moves farther from the nominal room temperature impedance value.

The effects of the thermal expansion of the probe are not taken into account with this implementation. Therefore, the implementation of this calibration method is not suggested for obtaining accurate elevated temperature measurements.

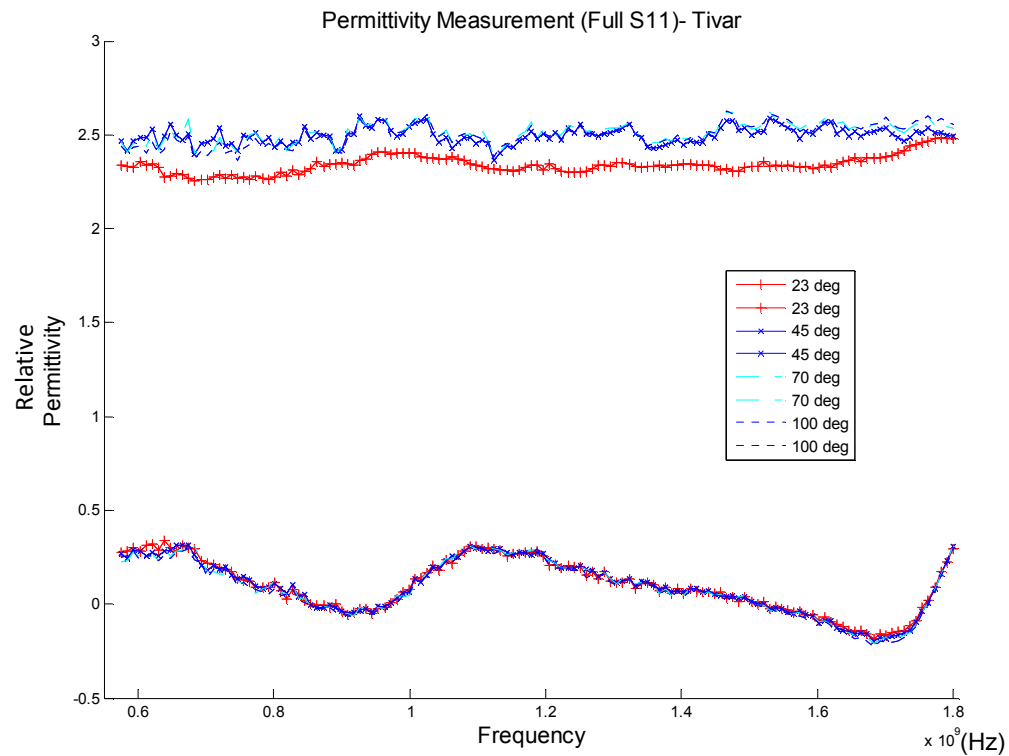


Figure 5.3 Relative Permittivity Extraction of Tivar at four temperatures using the Room Temperature Full S_{11} Calibration

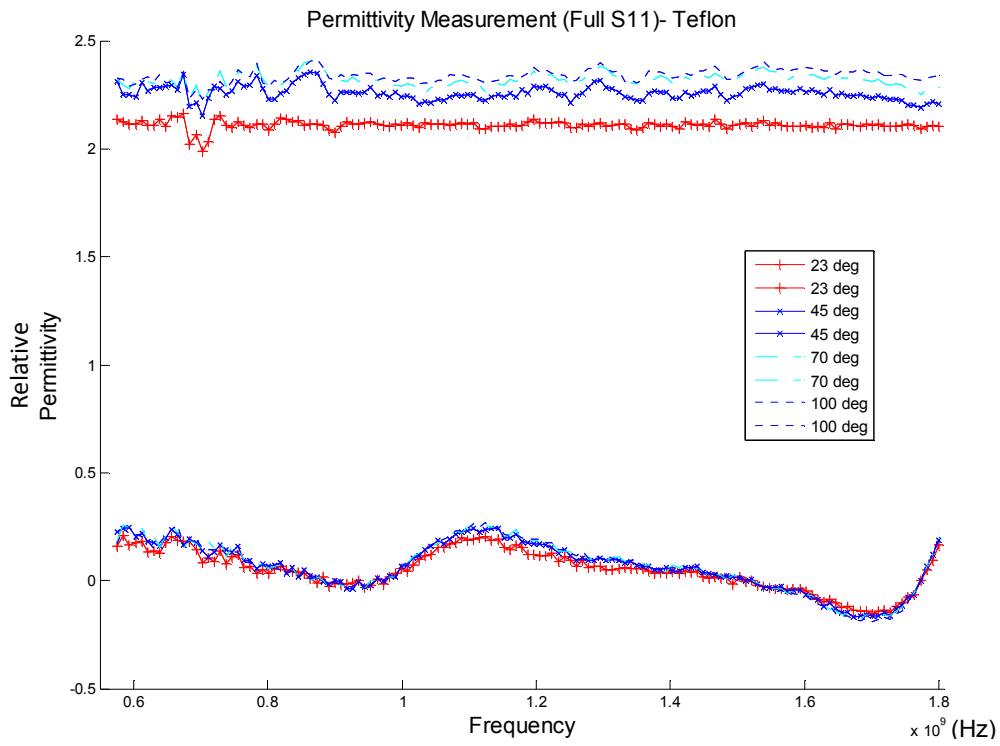


Figure 5.4 Relative Permittivity Extraction of Teflon at four temperatures using the Room Temperature Full S_{11} Calibration

Table 5.2 Relative Permittivity Value for Response Calibration (SL probe)

Response Calibration Styrofoam				
Temp. (°C)	Teflon		Polyethylene	
(23)	ϵ'_r 2.1 (<i>Stnd. Dev.</i>)	ϵ''_r 0.0003 (<i>Stnd. Dev.</i>)	ϵ'_r 2.3 (<i>Stnd. Dev.</i>)	ϵ''_r 0.0007 (<i>Stnd. Dev.</i>)
23	2.178 (0.0168)	-0.0186 (0.0305)	2.317 (0.0430)	-0.0107 (0.0250)
45	2.045 (0.0309)	-0.0174 (0.0302)	2.224 (0.0524)	-0.0340 (0.0378)
70	2.033 (0.0202)	0.0026 (0.0325)	2.230 (0.0377)	-0.0135 (0.0367)
100	1.950 (0.0181)	-0.0184 (0.0293)	2.024 (0.0389)	-0.0328 (0.03397)

The results obtained from the “Response” calibration (Table 5.2) behave as expected. The complex permittivity values decrease for both materials as temperature increases. The effects of thermal expansion still play a role in the error exhibited by this method, but it is expected that most of the error is from the calibration method. Figure 5.5 and Figure 5.6 show a plot of the “Response” calibration measurements taken at elevated temperatures. As temperature increases, the relative permittivity values of both materials decrease.

The effects of the thermal expansion of the probe are taken into account with this implementation, but the one term calibration method is not as accurate as a three term calibration method. The implementation of this calibration method can be used to obtain accurate elevated temperature measurements. It is important to note that the accuracy of this extraction technique could further be increased if a three term calibration technique could be used.

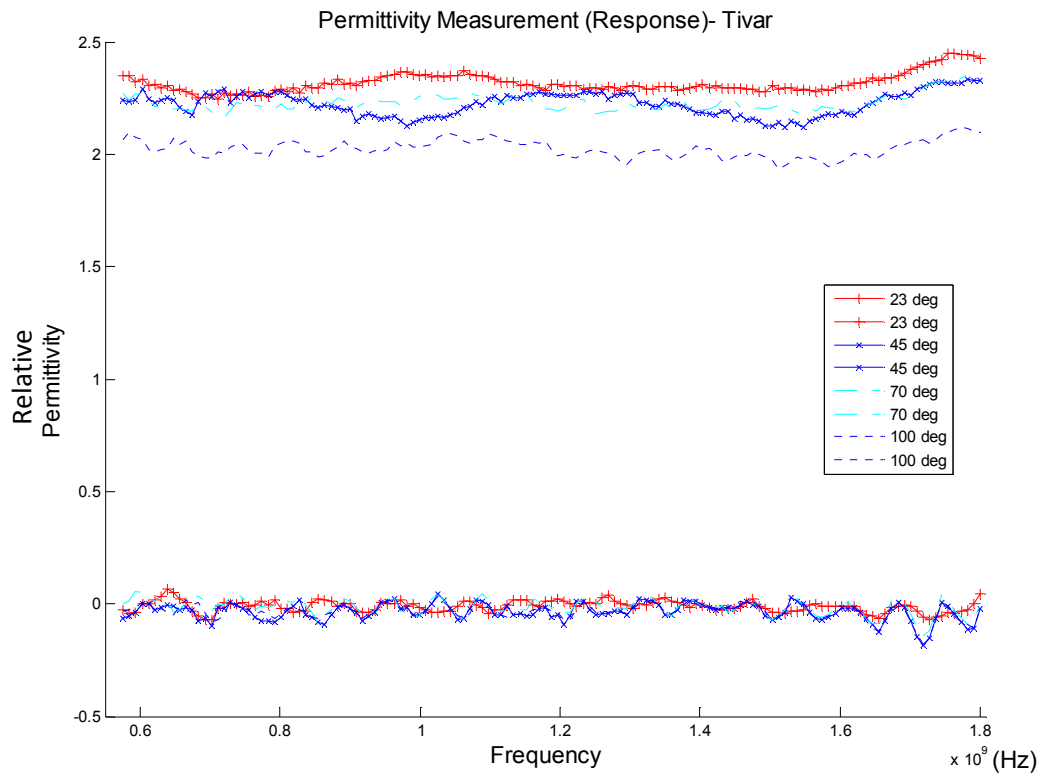


Figure 5.5 Relative Permittivity Extraction of Tivar at four temperatures using the Response Calibration

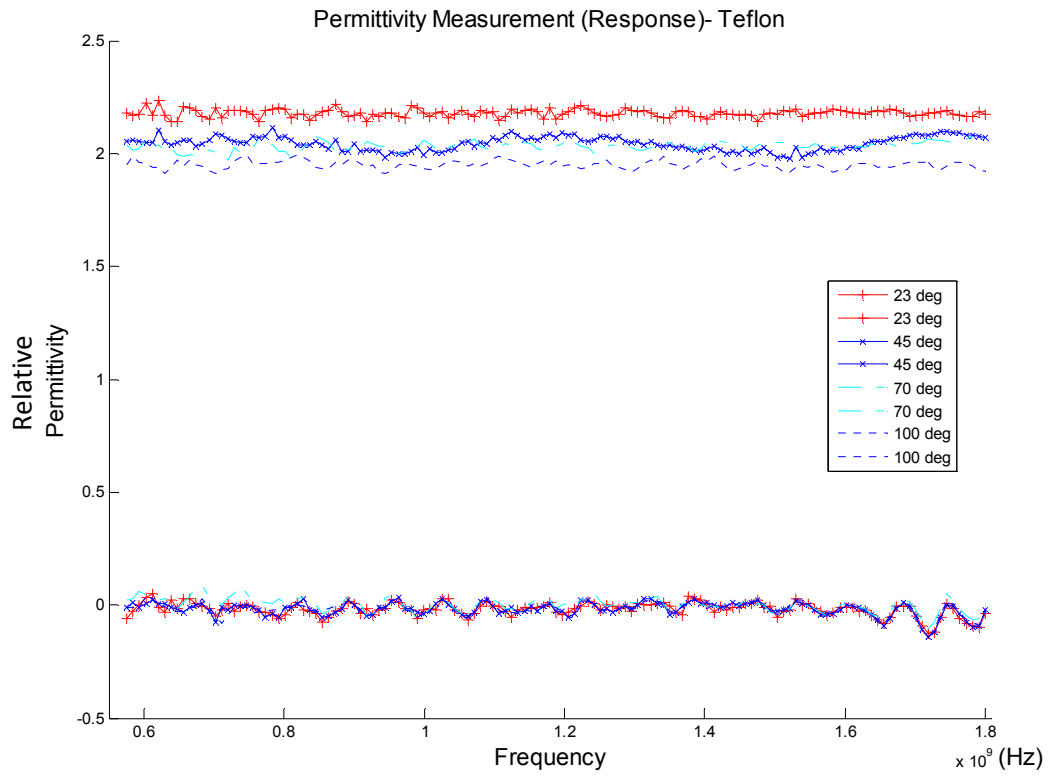


Figure 5.6 Relative Permittivity Extraction of Teflon at four temperatures using the Response Calibration

CHAPTER 6

CONCLUSIONS

6.1 Technique Summary

Three different open-ended coaxial probes were presented, and of these only one was used to extract the complex permittivity of an unknown material at elevated temperatures. The first probe or test probe is made from a highly polished- machined RF coaxial connector. It was used as a bench mark for future measurements. The second probe or stainless steel probe is made from stainless steel bars and a RF Clamp Type Connector. This probe was the motivation behind creating the final probe. The final probe or spring-loaded stainless steel probe is a variation of the original stainless steel probe. It enhances the original probe setup with the addition of a spring-loaded mechanism. It is the probe that is later used to test materials at elevated temperatures.

The probes are brought in contact with the tested material such that the fields at the probe end fringe into the material. After this arrangement is formed, complex permittivity is then extracted.

The lumped equivalent circuit capacitive model of the probe's fields fringing into a sample was used to extract the complex permittivity of materials using the open-ended coaxial probe. This approach was selected because of the relative ease of implementation as compared to other modeling techniques.

In order to increase accuracy of the solutions at elevated temperatures, the thermal expansion of the coaxial probe must be taken into account. This was done by performing a response calibration at each measurement temperature.

6.2 Future Work

This procedure served to give accurate material measurement results, but precision can be further increased in both the room temperature and elevated temperature measurements. The most immediate improvement that can be made lies in the equations for extracting the complex permittivity. The lumped equivalent circuit model of the probe's fields fringing into a sample degrades at higher frequencies, and it has been noted that measurements using a numerical computational method solution of the electromagnetic field equations suitable for a coaxial line open to a dielectric sample are generally more accurate (section 6.2.1). Also, further exploration into the calibration standards utilized provides another source of improvement to this technique. Lastly, gold plating the stainless steel probe will also enhance this technique.

6.2.1 Numeric solution for an open-ended coaxial probe

Perhaps a more accurate modeling method, to relate the load admittance as a function of the dielectric constant, is to implement a numerical computational method solution of the electromagnetic field equations suitable for a coaxial line open to a dielectric sample. The suggested approach for calculating a numerical solution of the electromagnetic field equations suitable for an open-ended coaxial line was introduced by D. K. Misra [23]. The model uses a quasi-static approximation which assumes that only the dominant TEM mode propagates inside the coaxial line.

Misra formulated a stationary relationship for the aperture input admittance using image theory and the boundary conditions of the tangential magnetic field equations as shown in (2.8):

$$Y_L = j \frac{k^2}{\pi \cdot k_{rp} \ln(b/a)} \int_a^b \int_a^b \int_0^\pi \cos \phi' \frac{\exp(-jkR)}{R} d\phi' d\rho' d\rho \quad (6.1)$$

where,

$$k = \sqrt{\epsilon \mu_0 \omega^2} \quad (6.2)$$

and

$$k_{rp} = \sqrt{\epsilon_{rp} \epsilon_0 \mu_0 \omega^2} \quad (6.3)$$

and

$$R = \sqrt{\rho^2 + \rho'^2 - 2\rho\rho' \cos \phi'} \quad (6.4)$$

where k is the wave number, k_{rp} is the wave number of the material inside the probe, and ω is the angular frequency; a and b are the inner radius and the outer radius of the probe,

respectively; ϵ_{rp} is the relative permittivity of the dielectric material inside the probe and ϵ is the total complex permittivity of unknown material under test (Figure 6.1).

The geometry of the probe end, as shown in Figure 6.2, shows the angles to and distance between source point S and the field point F, respectively; R is the distance between the source point and the field point; Φ is the angle between the field point and the x-axis; Φ' is the angle between the source point and the x-axis; ρ and ρ' are radial coordinates of F and S, respectively, at the aperture of coaxial probe [24].

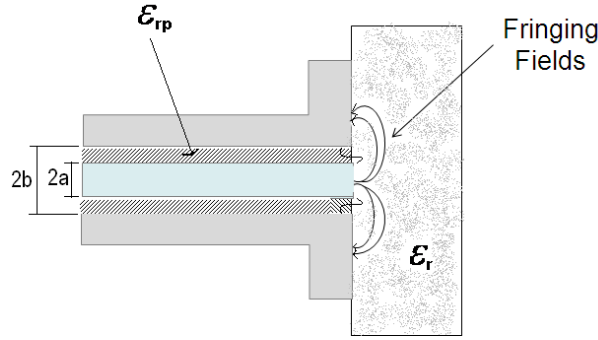


Figure 6.1 Open-ended coaxial probe in contact with material of relative complex permittivity, ϵ_r

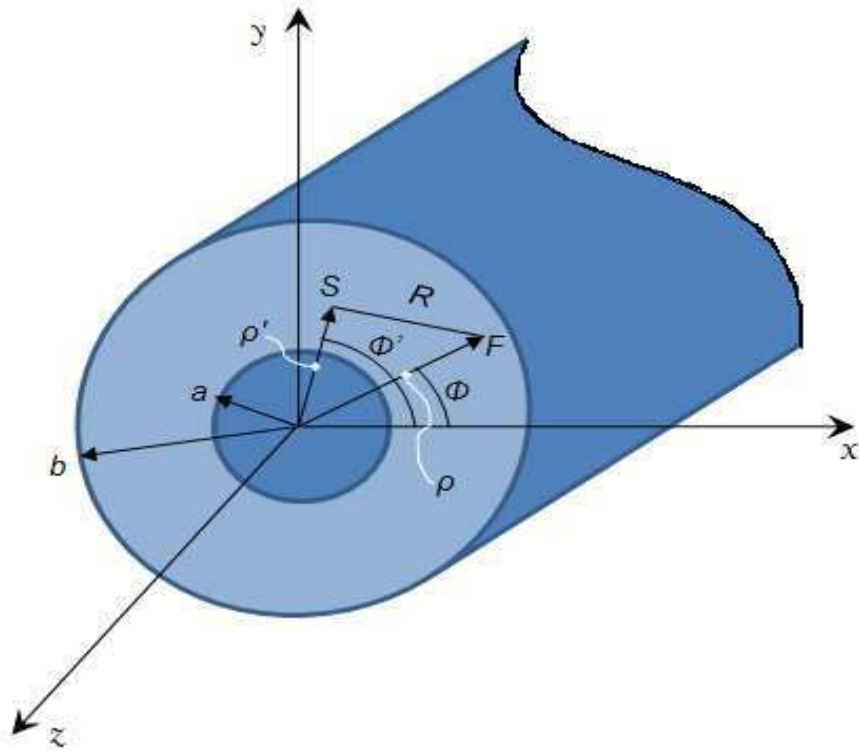


Figure 6.2 The probe tip geometry defining Equation (2.8). (Taken from An Open-ended Coaxial Probe for Broad-band Permittivity Measurement of Agricultural Products [24])

Assuming the coaxial opening is electrically very small, equation (6.1) can be approximated by the first few terms of the series expansion for the exponential term. The characteristic admittance Y_0 of the coaxial line can be obtained as follows:

$$Y_0 = \frac{2\pi}{\ln\left(\frac{b}{a}\right)\sqrt{\frac{\mu_0}{\epsilon_{rp}\epsilon_0}}} \quad (6.5)$$

and

$$Y_L = j \frac{2\omega\epsilon}{[\ln(b/a)]^2} \left[I_1 - \frac{k^2 I_3}{2} \right] + \frac{k^3 \pi \omega \epsilon}{12} \left[\frac{b^2 - a^2}{\ln(b/a)} \right]^2 \quad (6.6)$$

where

$$I_1 = \int_a^b \int_a^b \int_0^\pi \frac{\cos \phi'}{\sqrt{\rho^2 + \rho'^2 2\rho\rho' \cos \phi'}} d\phi' d\rho' d\rho \quad (6.7)$$

and

$$I_3 = \int_a^b \int_a^b \int_0^\pi \cos \phi' \left(\sqrt{\rho^2 + \rho'^2 2\rho\rho' \cos \phi'} \right) d\phi' d\rho' d\rho \quad (6.8)$$

The second term of the series expansion goes to zero on integration over Φ' and the fourth term reduces to the last term of (6.6). Under this condition, (6.6) reduces to

$$Y_L \approx \frac{j2\omega\epsilon}{[\ln(b/a)]^2} \left[I_1 - \frac{k^2}{2} I_3 \right] \quad (6.9)$$

I_1 and I_3 are integration constants which can be evaluated numerically for a given coaxial line, independent of the tested medium characteristics, and are dependent only on the physical dimensions of the aperture. A quadratic equation for the total complex permittivity, ϵ , can be formulated using (6.9) for a measured admittance Y_L . Likewise, the probe must be calibrated at the probe end in order to get accurate data [23].

6.2.2 Calibration Standards

The calibration standards are the main source of error, and the solution to this problem simply lies in establishing more accurate calibration standards. The short circuit can be better realized by using a conductive plastic polymer (i.e. Metal Rubber by NanoSonic). This will not only have the conductive properties of a short, but also be flexible enough to make sure an absolute short is obtained. The load calibration can be enhanced by manufacturing a square resistor (in Appendix A.3) that has a characteristic impedance of 50Ω . I would suggest the use of a resistive paste with a resistivity of $1 \Omega/\square$. If the final screen printed resistor value is lower than 50Ω , then this resistor can be filed down to increase the surface resistance or the $1 \Omega/\square$ resistive paste can be combined with a higher valued resistive paste until you reach the desired impedance (this will produce a better resistor). Better calibrations will help both room temperature and elevated temperature measurements.

For the elevated temperature set up, measurements calibrated with the probe and material under test at the measurement temperature and the reference material at room temperature will provide better elevated temperature measurements. In contrast, when the probe, material under test, and reference material are all calibrated at room temperature, measurements taken at elevated temperatures cause the system to drift. This system drift or phase error is caused by the thermal expansion of the probe [20]. A simple calibration at the desired temperature takes care of this problem. With better calibration standards for elevated temperature measurements, a Full-S₁₁ calibration can be taken at each temperature, as opposed to a less accurate Response calibration. Also, another solution to the thermal expansion problem with the probe would be to use a different conductive

material with a lower coefficient of thermal expansion (i.e. Kovar or a metalized ceramic).

6.2.3 Gold Plated Probe

Gold plating the outside of the center conductor and the inside of the pipe to a thickness of several skin depths would help with obtaining more accurate loss tangent measurements. From different Wikipedia pages, the thermal conductivity of gold at 100 °C is 312.0 W/(m°C) and the electrical conductivity of gold is 44.64×10^6 S/m (Table 6.1). Likewise, the thermal conductivity of stainless steel (316) at 100 °C is 16.20 W/(m°C) and the electrical conductivity of stainless steel (316) is 1.351×10^6 S/m (Table 6.1). This means that gold is 33 times more electrically conductive than stainless steel, making it the better conductor material to use for the probe. However, Table 6.1 also shows that gold is 19 times more thermally conductive than stainless steel.

Table 6.1 Thermal and Electrical Conductivities of Gold and Stainless

	Thermal Conductivity@ 100°C W/(m°C)	Electrical Conductivity S/m
Gold	312.0	44.64×10^6
Stainless Steel	16.20	1.351×10^6

Fortunately, since gold is such a good electrical conductor, it offers a good compromise even with the increased thermal conductance because the cross-sectional area over which it will conduct heat is very small. Given this small cross-sectional area, my calculations (Table 6.2) revealed a negligible amount of heat conducted by the gold.

The skin depth, δ , is equal to

$$\delta = 1/\sqrt{\pi f \mu \sigma_c} \quad (6.10)$$

where f is the frequency, μ is the permeability, and σ_c is the conductivity of the metal. When δ is small compared to the radius of the conductor, the AC resistance of the conductor is about equal to the DC resistance of a conductor with a cross-sectional area, A , equal to $2\pi r \cdot \delta$, where r is the radius of the conductor [25]. The total skin effect resistance [26], in (6.11), is equal to the series combination of the inner conductor resistance $R_{\delta a}$ and the outer conductor resistance $R_{\delta b}$.

$$R_\delta = R_{\delta a} + R_{\delta b} = \frac{L}{2\pi} \left(\frac{1}{a} + \frac{1}{b} \right) \frac{1}{\sigma_c \delta} \quad (6.11)$$

where

$$R_{\delta a} = \frac{1}{\sigma_c} \frac{L}{2\pi a \delta} \quad (6.12)$$

and

$$R_{\delta b} = \frac{1}{\sigma_c} \frac{L}{2\pi b \delta} \quad (6.13)$$

where L is the length of the coaxial line, a is the radius of the inner conductor, and b is the radius of the outer conductor.

The skin effect resistance [26] per unit length is equal to

$$R'_{\delta} = \frac{R_{\delta}}{L} = \frac{1}{2\pi} \left(\frac{1}{a} + \frac{1}{b} \right) \sqrt{\frac{\pi \mu}{\sigma_c}} \quad (6.14)$$

Therefore, the skin effect conductance per unit length is equal to

$$G'_{\delta} = \frac{1}{R_{\delta}} \cdot \frac{1}{L} = \frac{2\pi \cdot \sigma_c \delta}{\left(\frac{1}{a} + \frac{1}{b} \right)} \cdot \frac{1}{L^2} \quad (6.15)$$

and the total skin effect conductance, in (6.16), is equal to

$$G_{\delta} = \frac{1}{R_{\delta}} = \frac{2\pi \cdot \sigma_c \delta}{\left(\frac{1}{a} + \frac{1}{b} \right)} \cdot \frac{1}{L} \quad (6.16)$$

This total skin effect conductance is also the heat conducted by the gold plating as shown in Table 6.2.

Table 6.2 Calculations of Heat Conducted by Gold Plated probe

Skin depth@ 1 GHz

$$\delta = 1/\sqrt{\pi f \mu \sigma_c} = 9.010 \times 10^{-4} \text{ [m]}$$

Five skin depths thickness@ 1 GHz

$$\delta_{used} = 5 \cdot \delta = 45.05 \times 10^{-4} \text{ [m]}$$

For $\delta \ll a$ and $\delta \ll b$

Cross-sectional area

$$A_a = 2\pi \cdot a \cdot \delta_{used} = 1.121 \times 10^{-4} \text{ [m}^2]$$

$$A_b = 2\pi \cdot b \cdot \delta_{used} = 2.861 \times 10^{-4} \text{ [m}^2]$$

Inner conductor resistance@ L ≈ 12in = 0.3048m

$$R_{\delta a} = \frac{1}{\sigma_c} \frac{L}{A_a} = 8.709 \text{ [\Omega]}$$

Outer conductor resistance@ L ≈ 12in = 0.3048m

$$R_{\delta b} = \frac{1}{\sigma_c} \frac{L}{A_b} = 3.414 \text{ [\Omega]}$$

Total skin effect resistance

$$R_\delta = R_{\delta a} + R_{\delta b} = 12.12 \text{ [\Omega]}$$

Skin effect resistance per meter@ L ≈ 12in = 0.3048m

$$R'_\delta = \frac{R_\delta}{L} = 39.77 \text{ [\Omega/m]}$$

Thermal conductance per meter@ L ≈ 12in = 0.3048m

$$G'_\delta = \frac{1}{R_\delta} \cdot \frac{1}{L} = 0.2706 \text{ [S/m]}$$

Heat conducted by gold plated probe

$$G_\delta = \frac{1}{R_\delta} = 0.0825 \text{ [S]}$$

(negligible)

6.3 Conclusions

The open-ended coaxial probe method is a good approach when quick permittivity measurements are desired. This method is most used with liquids, but with the addition of the spring-loaded mechanism it serves as a good measurement system for solids as well. The response calibration offers a quick calibration that is relatively accurate. When measuring solids, an “Open” response calibration proves to work best, likewise when measuring liquids the short “Short” response calibration appears to work better. If elevated temperature measurements are desired, a three-term “Full-S₁₁” calibration at each measurement temperature will provide the most accurate results.

REFERENCES

- [1] H. Thomas, D. J. Elton, L. Riggs, S. Adanur, "Electronic Transmission and Reinforcement Fabric," National Textile Center Briefs, NTC Project: F05-Ae13, Jun. 2007
- [2] J. Baker-Jarvis, M. D. Janezic, J. H. Grosvenor, Jr., R. G. Geyer, "Transmission/Reflection and Short-Circuit Line Methods for Measuring Permittivity and Permeability," Boulder, Co: NIST Technical Note 1355, 1992.
- [3] Hewlett Packard, "HP Electronic Materials Measurement Seminar: A Broad Spectrum of Solutions for Materials Characterization," Hewlett Packard 5989-1075E
- [4] D. K. Ghodgaonkar, V. V. Varadan, "Free Space Measurement of Complex Permittivity and Complex Permeability of Magnetic Materials at Microwave Frequencies," IEEE Trans. Instrum. Meas., Vol. 39, pp. 387–394, Apr. 1990.
- [5] D. K. Ghodgaonkar, V. V. Varadan, V. K. Varadan, "A Freespace Method for Measurement of Dielectric Constants and Loss Tangents at Microwave Frequencies," IEEE Trans. Instrum. Meas., Vol. 38. pp. 789-793, 1989.
- [6] B. J. Wolfson, S. M. Wentworth, "Complex Permittivity and Permeability Measurement Using A Rectangular Waveguide," Microwave Opt. Techn. Lett., Vol. 27, No. 3, 180–182, Nov. 2000.
- [7] C. A. Jones, "Permeability and Permittivity Measurements Using Stripline Resonator Cavities: A Comparison," IEEE Trans. Instrum. Meas., Vol. 48, pp. 843–848, Aug. 1999.

- [8] Agilent Application Note, “Agilent Basics of Measuring the Dielectric Properties of Materials,” Agilent Literature Number 5989-2589en, Jun. 2006
- [9] T. T. Grove, M. F. Masters, R. E. Miers, “Determining Dielectric Constants Using A Parallel Plate Capacitor,” Am. J. Phys., Vol. 73, No. 1, Jan. 2005
- [10] M. N. O. Sadiku, Elements of Electromagnetics (2nd Ed). pp. 225-226. Saunders, Fort Worth, 1994.
- [11] Keqian Zhang, Dejie Li, Electromagnetic Theory for Microwaves and Optoelectronics (2nd Ed). pp. 270-272. Springer-Verlag Berlin Heidelberg, 2008
- [12] J. P. Grant, R. N. Clarke, G. T. Symm, N. M. Spyrou, “A Critical Study of The Open-Ended Coaxial-Line Sensor Technique for RF and Microwave Complex Permittivity Measurements,” J. Phys. E: Sci. Instrum., Vol. 22, 757-770, 1989
- [13] M. A. Stuchly, S. S. Stuchly, “Measurement of Radio Frequency Permittivity of Biological Tissues with an Open-Ended Coaxial Line: Part I - Part II,” IEEE Tran. Microw. Theory Tech., Vol. 82, No. 1, 82-92, 1982
- [14] M. A. Stuchly, S. S. Stuchly, “Coaxial Line Reflection Methods for Measuring Dielectric Properties of Biological Substances at Radio and Microwave Frequencies-A Review,” IEEE Trans. Instrum. Meas., Vol. 29, No. 3, 176-183, 1980.
- [15] D. Berube, F. M. Ghannouchi, P. Savard, “A Comparative Study of Four Open-ended Coaxial Probe Models for Permittivity Measurements of Lossy Dielectric/Biological Materials at Microwave Frequencies,” IEEE Tran. Microw. Theory Tech., Vol. 44, No. 10, 1928-1934, 1996
- [16] R. F. Harrington, Time-Harmonic Electromagnetic Fields, McGraw-Hill, Inc., New York, pp. 72, 455, 1961
- [17] B. Riddle, J. Baker-Jarvis, J. Krupka, “Complex Permittivity Measurements of Common Plastics Over Variable Temperatures,” IEEE Tran. Microw. Theory Tech., Vol. 51, No. 3, pp. 727–733, Mar. 2003.

- [18] D. Gershon, J. P. Calame, Y. Carmel, T. M. Antonsen, Jr., "Open-Ended Coaxial Probe for High-Temperature and Broadband Dielectric Measurements," IEEE Tran. Microw. Theory Tech., Vol. 47, No. 9, pp. 1640–1648, Sep. 1999.
- [19] S. Bringhurst, M. F. Iskander, M. J. White, "Thin-Sample Measurements and Error Analysis of High-Temperature Coaxial Dielectric Probes," IEEE Tran. Microw. Theory Tech., Vol. 45, 12, pp.2073-2083, 1997.
- [20] A. Lord, "Advanced RF Calibration Techniques," Presentation, Cascade Microtech Europe, Apr. 2002
- [21] M. Sheffer, D. Mandler, "Why is Copper Locally Etched by Scanning Electrochemical Microscopy?," Journal of Electroanalytical Chemistry, Vol. 622, pp. 115–120, 2008
- [22] S. M. Wentworth, Applied Electromagnetics, Early Transmission Lines Approach, Wiley, 2007
- [23] D. K. Misra, "A Quasi-Static Analysis of Open-Ended Coaxial Lines," IEEE Tran. Microw. Theory Tech., Vol. 35, No.10, Oct. 1987
- [24] N. I. Sheen, I. M. Woodhead, "An Open-Ended Coaxial Probe for Broad-Band Permittivity Measurement of Agricultural Products," J. Agric. Engineering. Res., Vol. 74, 193-202, 1999
- [25] Koehler, Circuits and Networks, pp. 196, Excerpt from book found at <http://w8ji.com/skindepth.htm>, Skindepth, Litz wire, Braided conductors, and resistance, 2005
- [26] S. M. Wentworth, Fundamentals of Electromagnetics with Engineering Applications, Wiley, pp. 229, 2005

APPENDIX A

CALIBRATION STANDARDS OVERVIEW

Section A.1 addresses the calibration standards used for the “Open” calibration standard. Section A.2 addresses the calibration standards used for the “Short” calibration standard. Section A.3 addresses the calibration standards used for the “Load” calibration standard. It is important to note that these are the calibration standards used in this research, but data extraction is not limited to only these.

A.1 Open Calibration Standard

Air and Styrofoam were used as the “Open” calibration standard in this research. Both were chosen because of their close resemblance to the relative permittivity of a vacuum ($\epsilon_r = 1$). For air the relative permittivity is equal to 1.00054. For Styrofoam (Figure A.1) the relative permittivity is equal to 1.03.



Figure A.1 Styrofoam brand rectangular sheet

A.2 Short Calibration Standard

A brass plate (Figure A.2), a steel plate (Figure A.3), a short standard at the end of coaxial plumbing (Figure A.4), deionized water, distilled water, and salt-water mixtures were used as the “Short” calibration standard in this research. Each “Short” calibration standard was chosen because of their similar scattering parameters to that of an ideal short circuit. All water samples (Figure A.5) were at least 200 mL.



Figure A.2 Brass plate



Figure A.3 Steel plate from rectangular waveguide



Figure A.4 Short Standard connected at end
of coaxial connector plumbing



Figure A.5 Liquid used as Short Standard

A.3 Load Calibration Standard

A $50\ \Omega$ annular resistor (Figure A.6), a $50\ \Omega$ standard at the end of a chain of coaxial connector plumbing (Figure A.8), deionized water (Figure A.9), alcohol, anti-freeze, and a resistive square print (Figure A.10) were used as the “Load” calibration standard in this research. All liquid samples were at least 200 mL.

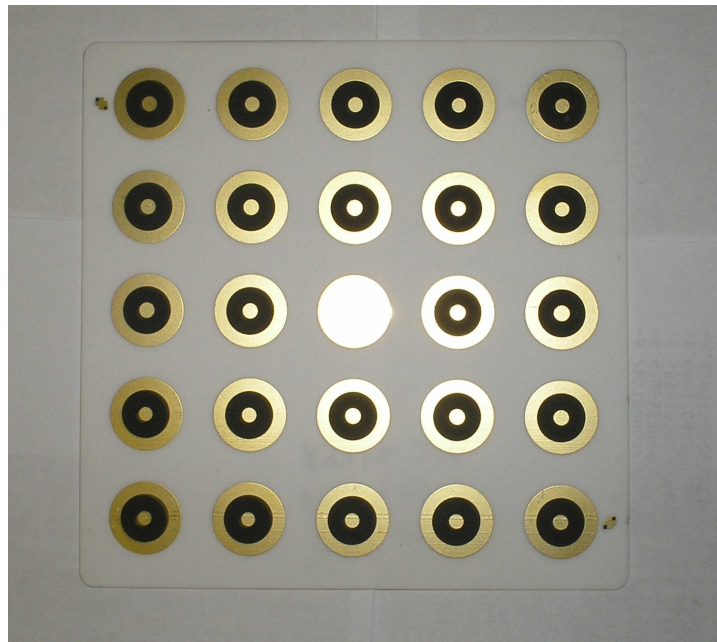


Figure A.6 $50\ \Omega$ Annular Resistor

The $50\ \Omega$ annular resistor (Figure A.5) ceramic sheet was created with multiple $50\ \Omega$ annular resistors such that all open-ended coaxial probes used in this work could fit any one resistive element. The actual resistors were created through a commercial fabrication process of screen printing, drying, and firing to apply the resistive material in between the gold conductors. The theory behind the annular resistor is listed below:

Annular Resistor

The annular resistor is a ring or circular shaped resistive element surrounded by a conductive material, where the inner and outer materials are very good conductors, relative to the annular material in between them. The fabrication of the annular resistor involved achieving both the correct resistive element to model a $50\text{-}\Omega$ characteristic

impedance and manufacturing a printed board of the inner and outer conductors made from gold.

The resistance of an annular resistive film (Figure A.7), R_{film} , depends on film resistivity, ρ , the natural logarithm of the ratio between the outer radius of the resistor, ‘b’, and inner radius of the resistor, ‘a’, and is reciprocally depended on the film thickness, t , as seen in equation (A.1).

Additionally, ‘a’ represents the radius of the conducting part of the tip, whereas ‘b’ is the radius of the entire tip including the insulation sheath [21].

$$R_{film} = \frac{\rho}{t} \cdot \frac{\ln(b/a)}{2\pi} \quad (\text{A.1})$$

where ρ/t is the sheet resistance, Rs .

In order to verify the validity of proposed 50- Ω characteristic impedance-annular resistor model, a similar derived formulation of a coaxial line with a conductive insulating material was found in Stuart Wentworth’s book called “*Applied Electromagnetics, Early Transmission Lines Approach*.” A detailed derivation of the annular resistor equation is shown below.

Derivation of annular resistance equation [22]

When finding the resistance, R, between the inner conductive element (radius a) and outer conductive element (radius b) for a specific thickness, t , of an annular resistive element filled with material of conductivity ' σ '. We can then assume two charges, $+Q$ and $-Q$, are placed on the conductive elements at radius ' a ' and ' b ', respectively, of an annular resistor (Figure A.6). By the use of Gauss's Law we can find the electric field intensity, \mathbf{E} , in equation (A.2) from the distributed charge across a field from $a \leq \rho \leq b$.

$$\mathbf{E} = \frac{Q}{2\pi\epsilon_0 t \rho} \mathbf{a}_\rho \quad (\text{A.2})$$

Then, using this field we can determine the potential difference between the inner and outer conductor as stated in equation (A.3)

$$V_{ab} = - \int_b^a \frac{Q}{2\pi\epsilon_0 t \rho} \mathbf{a}_\rho \cdot d\rho \mathbf{a}_\rho = \frac{Q}{2\pi\epsilon_0 t} \ln\left(\frac{b}{a}\right) \quad (\text{A.3})$$

Using the surface integral for a current through a surface and the point form of Ohm's Law, the current can then be found by the following as seen in equation (A.4)

$$\begin{aligned} I &= \int \mathbf{J} \cdot d\mathbf{S} = \int \sigma \mathbf{E} \cdot d\mathbf{S} \\ &= \int \sigma \frac{Q}{2\pi\epsilon_0 t \rho} \mathbf{a}_\rho \cdot \rho d\phi dz \mathbf{a}_\rho = \frac{\sigma Q}{2\pi\epsilon_0 t} \int_0^{2\pi} d\phi \int_o^t dz = \frac{\sigma Q}{\epsilon_0} \end{aligned} \quad (\text{A.4})$$

Finally, we must divide V_{ab} by I to find the resistance, as in equation (A.5)

$$R_{film} = \frac{1}{2\pi t\sigma} \ln\left(\frac{b}{a}\right) \quad (\text{A.5})$$

where conductivity, σ , is the inverse of resistivity, ρ . Equation (5) can then be rewritten as an equivalent expression to equation (1) by revising it in terms of the sheet resistance, R_s (Ω/\square), as in equation (A.6).

$$R_{film} = \frac{R_s}{2\pi} \ln\left(\frac{b}{a}\right) \quad (\text{A.6})$$

Fabrication

A MATLAB code was generated in order to calculate the correct sheet resistance. After the desired sheet resistance was established, the next step was to obtain the corresponding resistive pastes. The resistive paste samples were donated by Heraeus Materials Technology, LLC.

The fabrication of the annular resistors involved getting both the correct resistive element to model a $50\text{-}\Omega$ impedance and manufacturing a screen printed board of the inner and outer conductors made from gold. Michael Palmer performed most fabrication work for the annular resistors.

The gold inner and outer conductors were printed first followed by the commercial fabrication process of screen printing, drying, and firing to apply the resistive material in between the gold conductors as depicted in Figure A.6. The fabricated annular resistors had to be filed down with a Dremel tool due to the uncertainty of the thicknesses applied during the screening printing process.



Figure A.8 Load Standard connected at end
of coaxial connector plumbing



Figure A.9 Liquid used as Load Standard

The resistive square print, referred to as the square resistor, (Figure A.10) was created using the same fabrication process as the 50Ω annular resistor. The square resistor also went through a commercial fabrication process of screen printing, drying, and firing to apply some resistive material onto a ceramic substrate. It was given the trivial name “square resistor” for its square geometry. The only differences between the square resistor and the 50Ω annular resistors are that (1) the apparent area available for the open-ended coaxial probes to contact is greater for the square resistor and (2) there are no metal contacts constraining the probes placement. As a result of these differences, the probe can be positioned anywhere on the resistive surface of the square resistor. Both the greater available apparent area for contact and the decreased calibration difficulty make the square resistor more ideal for the calibration process with the coaxial probes.

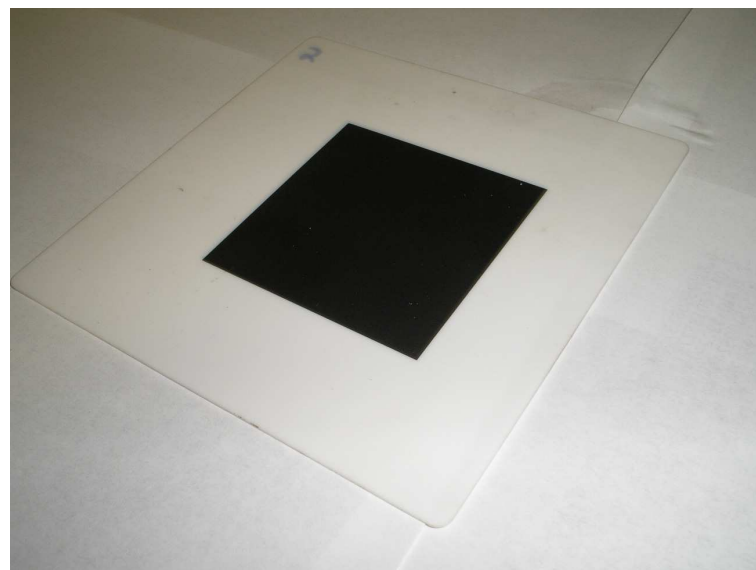


Figure A.10 Square Resistor (created using same fabrication process as 50Ω Annular Resistor)

APPENDIX B

TECHNIQUE DETAILS

The measurement process for the material characterization is relatively simple using the open-ended coaxial probe method. This section will describe the room temperature and elevated temperature calibration and measurement process. Also, the calibration materials will be explored in greater detail.

B.1 Room Temperature Measurement Procedure

Below are the steps necessary for obtaining permittivity measurements at room temperature using any open-ended coaxial probe.

1. Set up the VNA

- a. **Format**
 - i. More → Admittance chart
- b. **BW/Avg.**
 - i. Averaging → ON
 - ii. Avg. Factor → 16
- c. **Marker**
 - i. This step just displays a marker on screen

d. Start

i. 100 kHz

e. Stop

i. 1.8 GHz

2. Perform automatic calibration (*choose either “S₁₁ 1-port” or “Response”*)

a. Full S₁₁ 1-port

i. Cal

1. Correction → ON

2. Calibrate Menu → S₁₁ 1-port

ii. Pace probe flush against “Open” standard

1. Allow time for cable to stabilize

2. Press “Open”

a. For coax connector probe use Air or

Styrofoam

b. For spring-loaded probe use Styrofoam as

open

iii. Pace probe flush against “Short” standard

1. Allow time for cable to stabilize

2. Press “Short”

a. For coax connector probe use metal plate or

water

- b. For spring-loaded probe use metal plate
- iv. Pace probe flush against “Load” standard
 - 1. Allow time for cable to stabilize
 - 2. Press “Load”
- v. Press “DONE: 1-PORT CAL”

b. Response

- i.
- 1. Correction → ON
- 2. Calibrate Menu → Response
- 3. Choose either “Open” or “Short”
- ii. Pace probe flush against “Open” standard
 - 1. Allow time for cable to stabilize
 - 2. Press “Open”
 - a. For coax connector probe use Air or Styrofoam
 - b. For spring-loaded probe use Styrofoam as open
- iii. Pace probe flush against “Short” standard
 - 1. Allow time for cable to stabilize
 - 2. Press “Short”
 - a. For coax connector probe use metal plate or water
 - b. For spring-loaded probe use metal plate

iv. Press “DONE: RESPONSE”

3. Measure reference material (*must use the different material for reference then used for calibration*)

a. Place probe flush against reference material

i. Allow time for cable to stabilize

b. Press SAVE

i. Data only → Save ASCII

1. Disk must be loaded

4. Measure material under test

a. Place probe flush against material under test

i. Allow time for cable to stabilize

b. Press SAVE

i. Data only → Save ASCII

1. Disk must be loaded

B.2 Elevated Temperature Measurement Procedure

Below are the steps necessary for obtaining permittivity measurements at elevated temperatures using any open-ended coaxial probe.

1. Set up furnace (*NOTE: furnace overshoots desired temperature*)

a. Insert stopper over probe and insert in top over furnace

- b. Insert fire bricks and material under test to desired height of probe tip
- c. Turn furnace ON

2. Set up the VNA

- a. Format
 - i. More → Admittance chart
- b. BW/Avg.
 - i. Averaging → ON
 - ii. Avg. Factor → 16
- c. Marker
 - i. This step just displays a marker on screen
- d. Start
 - i. 100 kHz
- e. Stop
 - i. 1.8 GHz

3. Perform automatic calibration (choose either “ S_{11} 1-port” or “Response” or “Load” saved calibration)

a. Full S_{11} 1-port

- i. Cal
 - 1. Correction → ON

2. Calibrate Menu → S₁₁ 1-port
 - ii. Pace probe flush against “Open” standard
 1. Allow time for cable to stabilize
 2. Press “Open”
 - a. For coax connector probe use Air or Styrofoam
 - b. For spring-loaded probe use Styrofoam as open
 - iii. Pace probe flush against “Short” standard
 1. Allow time for cable to stabilize
 2. Press “Short”
 - a. For coax connector probe use metal plate or water
 - b. For spring-loaded probe use metal plate
 - iv. Pace probe flush against “Load” standard
 1. Allow time for cable to stabilize
 2. Press “Load”
 - v. Press “DONE: 1-PORT CAL”
- b. Response**
 - i.
 1. Correction → ON
 2. Calibrate Menu → Response
 3. Choose either “Open” or “Short”

- ii. Pace probe flush against “Open” standard
 - 1. Allow time for cable to stabilize
 - 2. Press “Open”
 - a. For coax connector probe use Air or Styrofoam
 - b. For spring-loaded probe use Styrofoam as open
- iii. Pace probe flush against “Short” standard
 - 1. Allow time for cable to stabilize
 - 2. Press “Short”
 - a. For coax connector probe use metal plate or water
 - b. For spring-loaded probe use metal plate
- iv. Press “DONE: RESPONSE”

c. Load saved Calibration

- i. Load disk with saved calibration routine
- ii. Recall
 - 1. Choose file “_____filename_____”

4. Measure reference material (must use the different material for reference then used for calibration)

- a. Place probe flush against reference material
 - i. Allow time for cable to stabilize
- b. Press SAVE

- i. Data only → Save ASCII

- 1. Disk must be loaded

5. Measure material under test

- a. Place probe flush against material under test

- i. Allow time for cable to stabilize

- b. Press

- i. Data only → Save ASCII

- 1. Disk must be loaded

APPENDIX C

MATLAB CODE

C.1 Lump Equivalent Circuit Model Code

```
% This program reads Filename of text file of reference material (Filename_ref.txt),  
% Filename of text file of material under test (Filename_MUT.txt), and Dielectric  
% constant of reference material (K_ref) and solves for the Reflection Coefficient of the  
% reference material (Gam_Ref), Reflection Coefficient of the material under test  
% (Gam_Meas), the real relative permittivity (er_real) of the material under test, and the  
% imaginary relative permittivity (er_imag) of the material under test  
  
%-----  
% If necessary program can also read the Reflection Coefficient of the Open  
% calibration standard (GamCal_O), Reflection Coefficient of the Short  
% calibration standard (GamCal_S), Reflection Coefficient of the Load  
% calibration standard (GamCal_L) and apply a de-embedding algorithm  
%-----  
  
% INPUTS  
% Filename_ref.txt - Filename of reference material  
% Filename_MUT.txt - Filename of material under test  
% K_ref - Dielectric constant of reference material (should be a  
% material of known relative permittivity)  
  
% number of rows to be used from loaded file (65 corresponds to 550 MHz  
% and 201 corresponds to 1.8 GHz)  
int = 65:201;  
  
% load reference material data  
load Filename_ref.txt % insert name of reference material file  
reload= Filename_ref(:,1:3);
```

```

% load material under test data
load Filename_MUT.txt % insert name of material under test file
MUTload= Filename_MUT(:,1:3);

% frequency loaded from reference material
f= refload(int,1);

% radian frequency
w=2*pi.*f;

% Separates reference material reflection coefficient into a real and
% imag component
S11_ref_r = refload(int,2); % real component of Reference Material S11
S11_ref_i = refload(int,3); % imaginary component of Reference Material S11

% calculate reflection coefficient of reference material
Gam_Ref = S11_ref_r - 1i*S11_ref_i;

%-----
% Insert 1-port de-embedding HERE for "reference material" if necessary
%-----

% Separates material under test reflection coefficient into a real and
% imag component
S11_MUT_r = MUTload(int,2); % real component of Material under test S11
S11_MUT_i = MUTload(int,3); % imaginary component of Material under test S11

% calculate reflection coefficient of material under test
Gam_MUT = S11_MUT_r - 1i*S11_MUT_i;

%-----
% Insert 1-port de-embedding HERE for "material under test" if necessary
%-----


% characteristic impedance (50 ohms)
Zo = 50;

```

```

% characteristic admittance (0.2 ohms^-1)
Yo = 1/Zo;

% magnitude of reflection coefficient of reference material
Gamref_Mag = abs(Gam_Ref);

% Phase of reflection coefficient of reference material (in degrees)
Gamref_Phase =(180/pi).*angle(Gam_Ref);

% capacitance orginating from sample fringing field
Cs = (sind(Gamref_Phase).*Gamref_Mag.*(-2))./...
(w.*Zo.*K_ref.*(1+Gamref_Mag.*cosd(Gamref_Phase).*(2)+(Gamref_Mag).^2));

% capacitance orginating from probe fringing field
Cp=(-2.*Gamref_Mag.*sind(Gamref_Phase))./...
(w.*Zo.*(1+2.*Gamref_Mag.*cosd(Gamref_Phase)+(Gamref_Mag).^2)) - K_ref.*Cs;

% magnitude of reflection coefficient of material under
GamMUT_Mag = abs(Gam_MUT);

% phase of reflection coefficient of material under
GamMUT_Phase =(180/pi).*angle(Gam_MUT);

% calculate real relative permittivity (er) of the material under test
er_real= (2.*GamMUT_Mag.*sind(-GamMUT_Phase))./...
(w.*Cs.*Zo.*(GamMUT_Mag.^2 + 2.*GamMUT_Mag.*cosd(GamMUT_Phase)+1))...
- Cp./Cs;

% calculate imaginary relative permittivity (err) of the material under test
er_imag = (1-GamMUT_Mag.^2)/(w.*Cs.*Zo.*(GamMUT_Mag.^2 ...
+ 2.*GamMUT_Mag.*cosd(GamMUT_Phase)+1));

```

C.1.a 1-Port De-embedding Algorithm

```

%%% -----USE ONLY IF 1-PORT DE_EMBEDDING IS WANTED -----
%%% reflection coefficient of (open) calibration termination
% load Open_CAL.TXT
% dtc2 = Open_CAL(:,1:3);

```

```

% CAL_O_r = dtc2(int,2);
% CAL_O_i = dtc2(int,3);
%
%%% reflection coefficient of (short) calibration termination
% load Short_CAL.TXT
% dtc1 = Short_CAL(:,1:3);
% CAL_S_r = dtc1(int,2);
% CAL_S_i = dtc1(int,3);
%
%%% reflection coefficient of (load) calibration termination
% load Load_CAL.TXT
% dtc3 = Load_CAL(:,1:3);
% CAL_L_r = dtc3(int,2);
% CAL_L_i = dtc3(int,3);
%
%%% CORRECTION METHOD
% MO = CAL_O_r - 1i * CAL_O_i;
% MS = CAL_S_r - 1i * CAL_S_i;
% ML = CAL_L_r - 1i * CAL_L_i;
% SO = 1;
% SS = -1;
% SL = 0;
% K1 = ML - MS;    %(approx. 1)
% K2 = MS - MO ;   %(approx. -2)
% K3 = MO - ML ;   %(approx. 1)
% K4= SL*SS*K1 ;  %(approx. 0)
% K5= SO*SS*K2 ;  %(approx. 2)
% K6= SL*SO*K3;   %(approx. 0)
% K7=SO*K1 ;       % (approx. 1)
% K8=SL*K2 ;       % (approx. 0)
% K9=SS*K3;        % (approx. -1)
% D1 = K4 + K5 + K6; % (approx. 2)
% a1= (MO.*K7 + ML.*K8 + MS.*K9)./D1; % (approx. 1)
% b1= (MO.*K4 + ML.*K5 +MS.*K6)./D1; % (approx. 0)
% c1 = (K7 + K8 + K9)./D1; % (approx. 0)
%
%%% Correction for reference material
% GM1 = Gam_Ref;
% GA1 = (GM1 - b1)./(a1 - c1.*GM1);
% Gam_Ref = GA1;
%
%%% Correction for material under test
% GM2 = Gam_MUT;
% GA2 = (GM2 - b1)./(a1 - c1.*GM2);
% Gam_MUT = GA1;
% -----

```

C.2 Numerical Method Extraction Code

The numerical method extraction algorithm presented did not accurately relate the reflection coefficient of a material under test to the complex permittivity of that tested material. This algorithm is only shown so that further work may be carried out on this code.

```
% This program reads Filename of text file of reference material
% (Filename_ref.txt), Filename of text file of material under test
% (Filename_MUT.txt), Filename of text file of open calibration standard
% (Filename_OpenCAL.txt), Filename of text file of short calibration
% standard (Filename_ShortCAL.txt), Filename of text file of load
% calibration standard (Filename_LoadCAL.txt), the diameter of the inner
% conductor of the used probe (a), the diameter of the outer conductor of
% the used probe (b) and solves for the real relative permittivity
% (er_real) of the material under test, and the imaginary relative
% permittivity (er_imag) of the material under test

% INPUTS
% Filename_ref.txt - Filename of reference material
% Filename_MUT.txt - Filename of material under test
% Filename_OpenCAL.txt - Filename of text file of open calibration
% standard
% Filename_ShortCAL.txt - Filename of text file of short calibration
% standard
% Filename_LoadCAL.txt - Filename of text file of load calibration
% standard
% a - diameter of the inner conductor of the used probe (in inch)
% b - diameter of the outer conductor of the used probe (in inch)

% load reference material data
load Filename_ref.txt % insert name of reference material file
reload= Filename_ref(:,1:3);

% load reference material data
load Filename_MUT.txt %insert name of material under test file
MUTload= Filename_MUT(:,1:3);
```

```

% load reflection coefficient of (open) calibration termination
load Open_CAL.TXT
dtc2 = Open_CAL(:,1:3);

% load reflection coefficient of (short) calibration termination
load Short_CAL.TXT
dtc1 = Short_CAL(:,1:3);

% load reflection coefficient of (load) calibration termination
load Load_CAL.TXT
dtc3 = Load_CAL(:,1:3);

% frequency loaded from reference material
f = refload(int,1);

% radian frequency
w=2*pi.*f;

% Separates reference material reflection coefficient into a real and
% imag component
S11_ref_r = refload(int,2); %real component of Reference Material S11
S11_ref_i = refload(int,3); %imaginary component of Reference Material S11

% calculate reflection coefficient of reference material
Gam_Ref = S11_ref_r - 1i*S11_ref_i;

% Separates material under test reflection coefficient into a real and
% imag component
S11_MUT_r = MUTload(int,2); %real component of Material under test S11
S11_MUT_i = MUTload(int,3); %imaginary component of Material under test S11

% calculate reflection coefficient of material under test
Gam_MUT = S11_MUT_r - 1i*S11_MUT_i;

% Separates open calibration reflection coefficient into a real and
% imag component
CAL_O_r = dtc2(int,2);
CAL_O_i = dtc2(int,3);

```

```

% calculate reflection coefficient of open calibration
GamCAL1_O = CAL_O_r -1i*CAL_O_i;

% Separates short calibration reflection coefficient into a real and
% imag component
CAL_S_r = dtc1(int,2);
CAL_S_i = dtc1(int,3);

% calculate reflection coefficient of short calibration
GamCAL2_S = CAL_S_r -1i*CAL_S_i;

% Separates load calibration reflection coefficient into a real and
% imag component
CAL_L_r = dtc3(int,2);
CAL_L_i = dtc3(int,3);

% calculate reflection coefficient of load calibration
GamCAL3_L = CAL_L_r -1i*CAL_L_i;

% speed of light
c=3e8;

% wavenumber
k = w./c;

% permittivity of free space
eps_0=8.854e-12;

% permeability of free space
mu_0=4*pi*10^-7;

eta=sqrt(mu_0/eps_0);

% freespace wavenumber
k0=w*sqrt(mu_0*eps_0);

% permittivity of dielectric inside probe
eps_c=2;

% characteristic admittance
Yo=2*pi/(log(b/a)*sqrt(mu_0/(eps_c*eps_0)));

```

% INTEGRATION

inTOcm =(1e-2/2.54); %converts from inches to centimeter
cmTOin =(2.54/1e-2); %converts from centimeter to inches

% outer diameter of probe

b= b*inTOcm;

% inner diameter of probe

a= a*inTOcm;

% integration functions

F = @(phiP,rhoP,rho) (cos(phiP))./(rho.^2 + rhoP.^2 - 2*rho.*rhoP.*cos(phiP)).^(1/2);
G = @(phiP,rhoP,rho) (cos(phiP)).*(rho.^2 + rhoP.^2 - 2*rho.*rhoP.*cos(phiP)).^(1/2);

% integration constants (triple integration)

I1 = triplequad(F,(.011),pi,a,b,a,b,[],@quadv);
I3 = triplequad(G,0,pi,a,b,a,b,[],@quadv);

%% CORRECTION METHOD

% % %Rho_m = is the measured reflection coefficient

% % %Gam_1 = the

% % %Gam_2 = the reflection coefficient of the standard 2 terminations used for calibration

% % %Gam_3 = the reflection coefficient of the standard 3 terminations used for calibration

% % %Rho_1 = the measured reflection coefficient corresponding to the calibration termination 1

% % %Rho_2 = the measured reflection coefficient corresponding to the calibration termination 2

% % %Rho_3 = the measured reflection coefficient corresponding to the calibration termination 3

% reflection coefficient of short standard used for calibration

Gam_1 = -1; %short

% reflection coefficient of open standard used for calibration

Gam_2 = 1; %open

% reflection coefficient of load standard used for calibration

Gam_3 = 0; %load

```

S11 = (Gam_1.*Gam_2.*Rho_3.*(Rho_1-Rho_2)+ Gam_1.*Gam_3.*Rho_2.*(Rho_3-
Rho_1)+ Gam_2.*Gam_3.*Rho_1.*(Rho_2-Rho_3))./(Gam_1.*Gam_2.*Rho_1-
Rho_2) ... + Gam_1.*Gam_3.*(Rho_3-Rho_1)+ Gam_2.*Gam_3.*(Rho_2-Rho_3));

S22 = (Gam_1.*(Rho_2-S11)+Gam_2.*(S11-Rho_1))./(Gam_1.*Gam_2.*Rho_2-
Rho_1));

S12nS21 = ((Rho_1-S11).*(1-S22.*Gam_1))./(Gam_1);

%true reflection coefficient
Gamma_true = (Rho_m-S11)./(S22.*Rho_m + S12nS21 - S11.*S22);
GamL= Gamma_true;

% constants for quadratic equation
const1= (1i.*w.^2)./((log(b/a))^2);
const2= const1.*(w.^2).*mu_0./2;
A=const2.*I3;
B=-const1.*I1;
C=(Yo.*(1-GamL)./(1+GamL));

% Correctionfactor (CF) is related to the reference material reflection
% coefficient
CF = ?????;

% Solved quadratic equation
X = (-B-sqrt(B.^2-4.*A.*C))/(2.*A)*(-CF);
% X = (-B-sqrt(B.^2-4.*A.*C))/(2.*A);

% the real relative permittivity (er_real) of the material under test
er_real = real(X);

% the imaginary relative permittivity (er_imag) of the material under test
er_imag = imag(X);

```